Deglacial and Holocene Sea ice and climate dynamics in the Bransfield Strait, at the Western Northern Antarctic Peninsula

Maria-Elena Vorrath[1], Juliane Müller[2,3,4], Paola Cárdenas[5], Thomas Opel[2], Sebastian Mieruch[2], Oliver Esper[2], Lester Lembke-Jene[2], Johan Etourneau[6,7], Andrea Vieth-Hillebrand[8], Niko Lahajnar[1], Carina B. Lange[5,9,10,11], Amy Leventer[12], Dimitris Evangelinos[7,13], Carlota Escutia[14], Gesine Mollenhauer[2,3]

[1]University Hamburg, Institute for Geology, Hamburg, Germany

[2]Alfred Wegener Institute, Helmholtz Centre for Polar and Marine Research, Bremerhaven, Germany

[3]MARUM – Center for Marine Environmental Sciences, University of Bremen, Germany

[4]Department of Geosciences, University of Bremen, Germany

[5]Centro de Investigación Dinámica de Ecosistemas Marinos de Altas Latitudes (IDEAL), Universidad Austral de Chile, Valdivia, Chile

[6]EPHE/PSL Research University, France

[7]UMR 5805 EPOC, CNRS, Université de Bordeaux, France

[8]Helmholtz Centre Potsdam GFZ German Research Centre for Geosciences, Potsdam, Germany

[9]Centro Oceanográfico COPAS CoastalSur-Austral/COPAS-Coastal, Universidad de Concepción, Chile

[10]Departamento de Oceanografía, Universidad de Concepción, Chile

[11]Scripps Institution of Oceanography, La Jolla, CA 92037, USA

[12]Department of Earth and Environmental GeosciencesGeology, Colgate University, New York, USA

[13]Departament de Dinàmica de la Terra i de l'Oceàn, Universitat de Barcelona, Spain

[14]Instituto Andaluz de Ciencia de la tierra, CSIC-Univ. de Granada, Spain

Correspondence to: Juliane Müller, juliane.mueller@awi.de

Abstract

The reconstruction of past sea ice distribution in the Southern Ocean is crucial for an improved understanding of ice-ocean-atmosphere feedbacks and the evaluation of Earth system and Antarctic ice sheet models. The Western Antarctic Peninsula (WAP) is experiencing rapid a warming since the start of regular monitoring of the atmospheric tempterature in since the 1950ies. Tand the associated decrease in sea ice cover contrasts the trend of

30 growing sea ice extent in ~~eastern~~ East Antarctica. To reveal the long-term sea ice history at the Northern Antarctic

31 Peninsula (NAP)~~WAP~~ under changing climate conditions we examined a marine sediment core from the eastern

32 basin of the Bransfield Strait covering the last Deglacial and the Holocene. For sea ice reconstructions, we focused

33 on the specific sea ice biomarker lipid IPSO$_{25}$, a highly branched isoprenoid (HBI), and sea ice diatoms, whereas

34 a phytoplankton-derived HBI triene (C$_{25:3}$) and warmer open ocean diatom assemblages reflect predominantly ice-

35 free conditions. We further reconstruct ocean temperatures using glycerol dialkyl glycerol tetraether (GDGTs) and

36 diatom assemblages, and compare our sea ice and temperature records with published marine sediment and ice

37 core data. ~~Our results document a retreat of the WAP ice shelf from~~at 13.~~8~~9 ka BP ~~on~~ (before present). A

38 ~~m~~Maximum ~~sea~~ ice cover is observed during ~~at 12.9 ka BP indicating~~ the Antarctic Cold Reversal (13.8 ka - 13

39 ka BP), while~~,~~ seasonally ice-free conditions permitting (summer) phytoplankton productivity are reconstructed

40 for the late Deglacial and the early Holocene from 13 ka to 8.3 ka BP. ~~while a still extended but variable sea ice~~

41 ~~coverage characterized the core site during the early Holocene from 11.7 ka to 8.2 ka BP.~~ An overall decreasing

42 sea ice trend throughout the Middle Holocene ~~is accompanied by~~coincides with ~~a successive~~ summer ocean

43 warming and increasing phytoplankton productivity. The Late Holocene is characterized by a highly

44 variable~~unstable~~ (winter) sea ice ~~cover~~concentrations~~conditions~~ and a sustained decline in~~further~~ the duration

45 and/or concentration of spring sea ice ~~decline until 0.5 ka BP~~. Overall diverging trends in GDGT-based TEX86L

46 and RI-OH' SOTs are found to be linked to opposing spring and summer insolation trends, respectively.

48 **Key Words**: Bransfield Strait~~Western Antarctic Peninsula~~, Holocene, sea ice cover, IPSO$_{25}$, highly branched

49 isoprenoids, diatoms, GDGTs

1 Introduction

51 Sea ice significantly affects the global climate system through its impact on the atmosphere-ocean exchange of

52 heat and gas, the physical and chemical properties of the water masses, ocean circulation, primary production and

53 biogeochemical cycles (Chisholm, 2000; Vancoppenolle et al., 2013). Sea ice cover limits evaporation, affects

54 precipitation and increases the reflection of solar radiation due to a high albedo (Allison et al., 1982; Butterworth

55 and Miller, 2016; Turner et al., 2017). When sea ice forms, cold and dense brines develop, contributing to the

56 formation of intermediate and deep waters (Nicholls et al., 2009). Importantly, the down-welling of these dense

57 water masses can prevent warm currents from reaching the continental ~~slope~~ shelf ~~where they stimulate the basal~~

58 ~~melt~~and stimulating basal melt of Antarctic ice shelves, with implications for the stability of ice sheets and

59 ~~eventually~~ global sea level (Cook et al., 2016; Escutia et al., 2019; Etourneau et al., 2019; Hellmer et al., 2012;

60 Huss and Farinotti, 2014). During the spring season, sea ice melting ~~stimulates~~ boosts marine primary production

61 by seeding algal cells, ~~the release of~~releasing nutrients and by promoting ocean stratification and a shallow mixed

62 layer depth (Arrigo et al., 1997; Vernet et al., 2008). In addition, nutrient supply can be locally enhanced by

63 ~~increasing~~ wind-driven upwelling activity along the sea ice edge~~, thus triggering phytoplankton blooms~~ (Alexander

64 and Niebauer, 1981). Enhanced carbon fixation through this ~~nutrient~~sea ice-stimulated biological pump hence

65 leads to an increase of biological material transport and organic carbon export to the ocean floor, thus ~~contributing~~

66 ~~to lower~~lowering surface pCO$_2$ (Han et al., 2019; Kim et al., 2004; Schofield et al., 2018; Wefer et al., 1988).

67 Since satellite-based sea-ice data became available in 1979, fast and profound changes have been observed both

68 in the Arctic ~~and~~as well as West Antarctica ~~globally due~~and ascribed to anthropogenic global warming (IPCC,

69 2021). The Western Antarctic Peninsula (WAP), in particular, is experiencing a rapid warming of the atmosphere

70 (Carrasco et al., 2021; Vaughan et al., 2003) and the ocean (Cook et al., 2016). This ~~is~~are accompanied~~is~~

71 ~~accompanied~~ by rapidly retreating glaciers and ice shelves (Cook et al., 2016; Rignot et al., 2019) and by

72 ~~significant~~ remarkable~~remarkably~~ loss of sea ice cover in the adjacent seas (Parkinson and Cavalieri, 2012).

73 For an assessment of the region's past sensitivity to climate change, the deglacial and Holocene climate history of

74 the Antarctic Peninsula (AP) has been studied extensively. The Deglacial, the transition from the Last Glacial

75 Maximum (LGM, Clark et al., 2012) to the Holocene, is characterized by a rapid warming punctuated by a distinct

76 cold event, the so-called Antarctic Cold Reversal (ACR) from 14.7 ka to 13 ka BP (EPICA Community Members,

77 2004; Mulvaney et al., 2012; Pedro et al., 2016). This drastic cooling of both atmosphere and ocean temperatures

78 in the high Southern latitudes is well reflected in ~~recorded by~~ stable isotope records of~~s in~~ Antarctic ice cores and

79 within marine sediments (Blunier and Brook, 2001; Domack et al., 2001; Jouzel et al., 1995; Morigi et al., 2003;

80 Stenni et al., 2001). From the Deglacial towards the Middle Holocene, the Antarctic Peninsula Ice Sheet (APIS)

81 retreated rapidly from the outer shelf to its modern configuration with ~~heavy~~high melt water discharge (Bentley

82 et al., 2014). Several ~~syntheses~~ comparisons between marine and lacustrine ~~of~~ Holocene climate records~~reflected~~

83 ~~in~~reflected ~~from marine and lake sediment cores~~ reveal that the timing of both hydrological and environmental

84 changes was ~~is~~ highly variable across~~at~~ the WAP (Allen et al., 2010; Ingólfsson et al., 2003; Minzoni et al., 2015;

85 Roseby et al., 2022; Sjunneskog and Taylor, 2002; Totten et al., 2022).~~The ice core records from James Ross~~

86 ~~Island (JRI) at the northeastern tip of the AP shows a pronounced warming between about 12 and 11 ka BP~~

87 ~~followed by a cooling trend until about 9 ka BP and stable temperatures until 2.5 ka BP. From 2.5 ka BP in the~~

88 ~~Late Holocene cooling was reversed since~~temperatures cooled until 0.6 ka BP (Mulvaney et al., 2012). An overall

89 consensus, however, is that WAP ocean temperature~~s~~ were~~in the WAP was~~, in comparison to the Deglacial or the

90 Late Holocene, warmer during the Early and Middle Holocene ~~Optimum~~, i.e. between 12 ka and 4 ka BP

91 (Shevenell et al., 2011). In contrast, marine sediment records show ~~many~~multiple different climate patterns for the

92 Late Holocene ~~shows many different climate patterns~~ around the AP, including a continuous Neoglacial cooling

93 (Etourneau et al., 2013)~~. whereas other records other studies resolve warmer and colder phases such as the~~

94 ~~Medieval Climate Anomaly and/or the Little Ice Age (Bentley et al., 2009)~~.

95 Knowledge of past Southern Ocean sea ice variability is crucial to~~for~~ accurately modell~~ing~~ climate feedbacks

96 ~~impacting the Antarctic ice sheet stability since the LGM~~ (Crosta et al., 2022). For periods beyond the satellite

97 era, information on past sea-ice conditions~~knowledge~~ is based on proxies from marine sediments, ~~and~~ ice cores

98 (*e.g.* Bracegirdle et al., 2015, 2019; Crosta et al., 2022; Escutia et al., 2019; Thomas et al., 2019), and snow petrel

99 stomach oil deposits (McClymont et al., 2022). At present, most climate m~~M~~odels, ~~however,~~ do~~ not only~~often fail

100 to reproduce ~~seasonal sea ice cycles~~observed sea ice trends of the satellite era; simulated sea ice

101 conditions~~reconstructions and observations of sea ice~~ for both glacial and interglacial periods ~~and~~ also often

102 disagree with geological proxies (Roche et al., 2012). Ice-core based sea ice reconstructions ~~for the LGM are~~

103 primarily use ~~based on~~ the concentrations of sea salt sodium (WAIS Divide Project Members, 2015). However,

104 since sea-salt aerosols might be overprinted by the highly variable wind direction and meteorological conditions

105 in Antarctica, ~~and thus not reflect~~sea salt records may not sufficiently ~~be consistent in~~ reflecting regional sea ice

106 conditions (Thomas et al., 2019). Although marine sediment records usually~~s mostly~~ have a lower temporal

107 resolution than ice cores, ~~they~~ marine proxy reconstructions can resolve regional and - depending on the spatial

108 distribution of sediment cores - of~~/or~~ large-scale changes in sea ice conditions, as well as sea surface and

109 subsurface ocean temperature, primary productivity and marine ecology (Hillaire-Marcel and de Vernal, 2007). In

110 addition to commonly used geochemical, lithological and microfossil proxies (*e.g.* ice rafted debris (IRD), diatom

111 assemblages, total organic carbon), new approaches focus on specific organic biomarkers - highly branched

112 isoprenoids (HBIs) - as ~~reliable~~ proxies to distinguish between open marine and seasonally sea ice covered

113 environments. The di-unsaturated HBI IPSO$_{25}$ (Ice Proxy for the Southern Ocean, C$_{25:2}$, Belt et al., 2016; Massé

114 et al., 2011) that is produced by sea ice algae and deposited on the ocean floor after the sea ice melt in spring has

115 already been applied ~~for~~ in Antarctic sea ice reconstructions (*e.g.* Barbara et al., 2013; Denis et al., 2010; Etourneau

116 et al., 2013). Following the phytoplankton-~~P~~PIP$_{25}$ sea-ice index (~~. ~~PIP$_{25}$~~.~~) approach for the Arctic (Müller et al.,

117 2011), IPSO$_{25}$ has been combined with phytoplankton-derived ~~ HBI trienes and/or sterols ~~phytoplankton~~ to

118 determine the phytoplankton-IPSO$_{25}$ sea ice index ~~called~~ PIPSO$_{25}$ (Vorrath et al., 2019), which has been

119 successfully evaluated with recent Antarctic spring sea ice concentrations (Lamping et al., 2021).~~.~~ Other studies

120 applied PIPSO$_{25}$ and examined its potential for sea ice reconstructions over ~~periods of~~ the industrial era (Vorrath

121 et al., 2020) and ~~over~~ deglacial and Holocene time intervals in ~~has been used in paleo sea ice studies from~~ the

122 Amundsen Sea (Lamping et al., 2020). ~~Hence, the combination to~~Ccombining these new molecular proxies with

123 the classical diatom assemblage approach and/or geochemical ice core proxies provides~~offers~~ a thorough

124 assessment of~~unique opportunity to robustly reconstruct~~ past sea ice conditions.~~at the WAP.…~~

125 Here, we present a marine sediment record covering the past 13.8~~9~~ ka BP and ~~to~~ reconstruct Deglacial and

126 Holocene environmental conditions in the eastern~~northern~~ Bransfield Strait at the NAP~~at the northernmost position~~

127 ~~of the WAP~~. Our study is based on a multiproxy approach focusing on the sea ice biomarker IPSO$_{25}$, an open

128 ocean marine phytoplankton biomarker (HBI triene), and on glycerol dialkyl glycerol tetraether lipids (GDGTs)

129 for subsurface ocean temperatures (SOT). Additional estimates~~information~~ of primary productivity, ~~about the~~

130 ~~probability of~~ winter sea ice coverage (WSI) and summer sea surface temperature (SSST) come~~s~~ from bulk

131 sediment organic carbon and biogenic silica contents and diatom assemblages using transfer functions,

132 respectively. In an intercomparison, we evaluate the different approaches to reconstruct sea ice conditions and

133 ocean temperatures. and~~We discuss We~~ ~~compare discuss and compare~~ our proxy results in regard of~~with~~ other

134 marine sediment and ice core records ~~spanning the Holocene~~ providing further insight into the environmental

135 dynamics at the Antarctic Peninsula ~~across the Deglacial and the Holocene~~.

136 **2   Material and Methods**

137 **2.1 Study Area**

138 The Bransfield Strait is located between the N~~W~~AP and the South Shetland Islands (SSI~~;)~~ (Fig. 1a), comprising a

139 trough~~t~~ (> 2000 m) ~~lying~~ between a narrow shelf to the north (SSI) and a broad shelf area to the south (AP). ~~Within~~

140 ~~this area, a shallow shelf and deeper depressions characterize the Bransfield Basin with water depths exceeding~~

141 ~~2000 m~~ (Fig. 1b). The shelf area~~s~~ w~~ere~~as affected by intense ice sheet dynamics during the last glaciation (Canals

142 and Amblas, 2016b; Ingólfsson et al., 2003) leaving ice sheet grounding lines and glacial troughs on the sea-floor

143 (Canals et al., 2016; Canals and Amblas, 2016a).

144 -   The modern Bransfield Basin is influenced by complex oceanic current systems.~~, which are not fully~~

145 ~~constrained because three different water masses enter the basin from the east and west (Moffat and Meredith,~~

146 ~~2018; Sangrà et al., 2011) and their mixing is not well understood. The C~~cold (< 0 °C) and relatively salty Weddell

147 Sea Water (WSW) enters from the east, flows alongshore the peninsula and fills the Bransfield Strait~~n~~ basins

148 below 150 m water depth~~surface~~. ~~The WSW is also observed   at greater depths (200-600 m) north of the SSI~~

149 ~~(outer shelf) and at Elephant Island due to wind driven modulation (Meijers et al., 2016).~~ In the western part of

150 the Bransfield Strait, the WSW mixes with warmer ~~a second water mass, the~~ Bellingshausen Sea Water (BSW; 0

151 - 50 m water depth) and Circumpolar Deep Water (CDR; 200 - 550 m water depth; Collares et al., 2018; Sangrà

152 et al., 2011, 2017), which areis transported in a branch of the Antarctic Circumpolar Current (ACC) over the

153 Anvers Shelf. It conveys well-stratified, fresh and warmer (> 0 °C) surface water to a depth of about 50 m (Sangrà

154 et al., 2011). A third water mass oAlso originating from the ACC is a third, deeper water mass, Originating from

155 the Circumpolar Deep Water (CDW), that is present between 200 m and 550 m (Sangrà et al., 2017). BSW and

156 CDW flow eastward along the SSI, turn around and flow westward at the northern tip of the islands (Sangrà et al.,

157 2011). BSW and WSW forms the subsurface Bransfield front with the CDW at depth and the surface Peninsula

158 Front (PF) with the WSW, that runs parallel to the Antarctic mainland (Sangrà et al., 2011, 2017). The interplay

159 of currents leads to a stratification of the water column ofpronounced pycnoclinte within the upper 20 m of the

160 water column in summer, with accompanied by a steep temperature gradient in the first upper 100 m, as below

161 sea surface. This can be observed in CTD hydrographic profiles fromin the Bransfield Basin that show a dominance

162 of WSW below 200 m (see Fig. 1c and Sangrà et al., 2011). The eddy system at the Peninsula Front is assumed to

163 play a key role for mixing and upwelling of the different surface and subsurface water masses (Sangrà et al., 2011;

164 Zhou et al., 2002), while several glaciers from the WAP influence coastal surface water due to meltwater discharge

165 and also transport dense bottom waters to the Bransfield Basin (Meredith et al., 2018).

166 Modern sea ice conditions at the core site in the eastern Bransfield Strait are characterized by a mean winter sea

167 ice concentration of ca. 50%, which declines to 18% and less than 2% sea ice concentration during spring and

168 summer, respectively (*cf.* Vorrath et al., 2019). Modern sea ice conditions follow a declining trend in all seasons

169 with a nearly sea ice free summers (Hobbs et al., 2016; Vorrath et al., 2020).While atmospheric temperatures show

170 a rising trend since the 1950ies ocean temperatures (Carrasco et al., 2021), ocean temperatures are increasingly

171 influenced by warm water intrusions and higher sea surface temperatures (Martinson and McKee, 2012; Meredith

172 and King, 2005). At the core site, mean annual sea surface temperatures are -0.6 °C with up to 0.8 °C during

173 summer (WOA 18; Boyer et al., 2018; Locarnini et al., 2018).

174 Primary production in the Bransfield Strait is mainly driven by mixing of water masses at the fronts (Gonçalves-

175 Araujo et al., 2015), mixed layer depth and upwelling (Sangrà et al., 2011), sea ice dynamics (Vernet et al., 2008)

176 and iron availability (Klunder et al., 2014). High concentrations of chlorophyll *a* and diatoms are distributed north

177 of the Peninsula FrontPF and at the SSI, while lower production and communities of nanoplanktonic plankton

178 nanoflagellates are found between the Peninsula Front and the WAP (Gonçalves-Araujo et al., 2015). Further,

179 changes in coastal primary production are driven by upwelling, elevated iron distribution availability, as well as

180 the nutrient release and surface water stratification generated by melting sea ice in the austral springand the retreat

181 of sea ice cover in spring releasing nutrients and stabilizing the water column (Vernet et al., 2008). A close robust

182 link between marine primary production at the surfacein surface waters and the sediment composition at the

Formatiert: Schriftart: Kursiv

183 underlying ocean floor is reflected in high concentrations of total organic carbon (TOC), pigments, sterols and

184 diatoms (Cárdenas et al., 2019), and supported by studies confirming high fluxes of sinking particles (Kim et al.,

185 2004; Wefer et al., 1988). In the study area, particle flux is highly variable with seasonal peaks occurring in late

186 spring, which accounts for 85% of the total flux (Ducklow et al., 2008). Lithologically, the sediments consist

187 mainly of terrestrial terrigenous silt and clay with varying amounts of diatom mud and ooze, and sand (Cádiz

188 Hernández, 2019; Lamy, 2016; Wu et al., 2019).

189

190 **2.2 Sediment samples and age model**

191 Piston core PS97/072-1 (62° 0.39' S, 56° 3.86' W, 1993 m water depth, 1583 cm in length) was recovered in the

192 eastern Bransfield Strait Basin during R/V *Polarstern* cruise PS97 (Lamy, 2016) (Fig. 1). The sedimentcore is

193 dominated by silt with thin layers of sand, clay, and traces of volcanic ash. Single pebbles are present below 630

194 cm. The core is disturbedSince we found disturbed sediments below 1015 cm depth and, we only considered

195 samples from above this level for our analyses. SAfter an XRF scan the core sampling for different analytical

196 approaches was done at the Alfred Wegener Institute (AWI) where the the samples were stored frozen in glass

197 vials (for biomarker analysis) and at 4 °C in plastic bags (for micropaleontology).

198 The age model of core PS97/072-1 is based on ^{14}C radiocarbon dating of eight calcite benthic foraminiferal and

199 mollusk fragments samples with the mini carbon dating system (MICADAS) available at AWI (Mollenhauer et

200 al., 2021). From the conventional ^{14}C age we subtracted a reservoir age based on modelling by Butzin et al. (2017)

201 and also subtracted an estimated ventilation age of 1200 years to account for the considerable water depth of our

202 site (see table supplement section 1), before we calibrated the ages with the calibration curve SHIntCal20 (Reimer

203 et al., 2020) (Hogg et al., 2020) to calendar years before present (cal BP) with Calib 7.1 (Stuiver et al., 2018). To

204 estimate the top age of the core top, TOC and biogenic opal data of the piston core were matched with data from

205 a multicore from the same sampling site that has been previously dated via ^{210}Pb (Vorrath et al., 2020; supplement

206 section 2). Ages of sediments below the oldest radiocarbon date (868.5 cm; 12.04 ka BP) were extrainterpolated

207 assuming a constant sedimentation rate.AThe downcore ages between the lowest radiocarbon dates sample and

208 the core bottom was interpolated based on previous sedimentation rates. We applied the Bayesian age modelling

209 tool *hummingage*, a freely available tool developed at AWI, that has been successfully applied in previous studies

210 (*e.g.* Ronge et al., 2021). As the lack of age constraints between 12 ka and 6 ka BP may introduce chronological

211 uncertainties, we only focus on overall trends reflected in our data and refrain from detailed allocations of known

212 climatic events in this older time period.

2.3 Organic geochemical analyses of piston core PS97/072-1

For the analyses of the bulkseveral organic geochemical compositioncomponents and biomarkers, the 334 sediments samples were freeze-dried and homogenized in an agate mortar. Prior to sediment homogenization, coarse grains were separated using a sieve (5 µm mesh size). Total carbon (C) and nitrogen (N) were measured with a CNS analyzer (Elementar Vario EL III, error of standards and duplicates < 5%). TOC was measured on 0.1 g of acidified samples (500 µl HCl) and determined in a carbon-sulphur determinator (CS-800, ELTRA, standard error < 0.6%). To identify the source of TOC, measurements of stable carbon isotopes of bulk organic matter were done at Universität Hamburg (UHH), Germany, and at Washington State University (WSU), USA. At UHH, the samples were acidified three times with 100 µl 1 N HCl and dried on a hotplate. High-temperature combustion was done in an Elementar CHNOS Vario isotope elemental analyser at 950 °C and the analysis was conducted with an Elementar IsoPrime 100 isotope ratio mass spectrometer. We calibrated the pure tank CO_2 with the International Atomic Energy Agency reference standards IAEA-CH6 and IAEA-CH7. These and two other standards (IVA Sediment and Sucrose) acted as internal standards in the measurement. The error of continuous standard duplicates was < 0.2‰ and <0.06‰ for sample duplicates. At WSU, 100 mg of freeze-dried sediment samples were used. An elemental analyzer coupled with an Isoprime isotope ratio mass spectrometer (IRMS) was used, with a precision of 0.1‰. The running standard was a protein hydrolysate calibrated against NIST standards. Isotope ratios are expressed in units per mil (‰). $\delta^{13}C$ values are expressed in ‰ against Vienna Pee Dee Belemnite (VPDB).

Biogenic opal was estimated on 327 samples following the alkaline extraction procedure described by Mortlock and Froelich (1989), but using 0.5M NaOH as a digestion solution (Müller and Schneider, 1993). Extraction and analysis by molybdate-blue spectrophotometry were conducted at the University of Concepción, Chile. Values are expressed as biogenic opal by multiplying the Si (%) by 2.4 (Mortlock and Froelich, 1989). Opal values could be somewhat overestimated by 2 - 2.5% since we We did not correct for the release of extractable Si from coexisting clay minerals, and thus biogenic opal values could be slightly overestimated (Schlüter and Rickert, 1998). Instrumental precision was ±0.5%; error of duplicates ≤ 3%). Details on the methodology used can be found in Cárdenas et al. (2019).

The extraction, purification and identification of 137 samples to identify HBIs followed the analytical protocol published e.g. in Belt et al. (2014) and Vorrath et al. (2019). Prior to extraction, 40 µl 7-hexylnonadecane (7-HND; 0.0019 µg/µl) and 100 µl C_{46} (0.0098 µg/µl) were addedserved as internal standards. Lipids were extracted using ultra sonication and a mixture of CH_2Cl_2:MeOH (v/v 2:1; 6 ml). HBIs and GDGTs were separated by means of open column chromatography using SiO_2 as the stationary phase and hexane, and CH_2Cl_2:MeOH (v/v 1:1) as

244 eluents. HBIs were analyzed by means of an Agilent 7890B gas chromatograph (30 m DB 1MS column, 0.25 mm

245 diameter, 0.250 µm film thickness) coupled to an Agilent 5977B mass spectrometer (MSD, 70 eV constant

246 ionization potential, ion source temperature 230 °C). The initial oven temperature of 60 °C was held for 3 min,

247 ramped to 325 °C within 23 min, and was held at 325 °C for 16 min. HBIs were identified *via* comparison of

248 their retention times (IPSO25 and HBI triene with RI 2084DB-1MS and 2046DB-1MS, respectively) and mass

249 spectra with published mass spectra (Belt, 2018) and quantified using the ratio of peak areas of individual HBIs

250 (m/z 346; m/z 348) and the 7-HND (m/z 266) standard and consideration of instrumental response factors. The

251 error of duplicates was <1.4% for IPSO$_{25}$, <2.6% for HBI trienes. The phytoplankton-IPSO$_{25}$ index (PIPSO$_{25}$) was

252 calculated after Vorrath et al. (2019) as:

253 $$PIPSO_{25} = \frac{IPSO_{25}}{IPSO_{25}+(c\times phytoplankton\ marker)} \quad . \tag{1}$$

254 The concentrations of the phytoplankton-derived HBI~~HBI~~ z-triene are ~~was is considered as a phytoplankton~~

255 ~~biomarker and, since the concentrations in these samples are~~were ~~on~~ at the same level as IPSO$_{25}$, and the c-factor

256 was hence set to 1 (Vorrath et al., 2019). To confirm the sea-ice origin of IPSO$_{25}$, the stable carbon isotope

257 composition of IPSO$_{25}$ was examined in 8 samples (with minimum 50 ng carbon) via GC-irm-MS at the GFZ

258 Potsdam, Germany. The GC (7890N Agilent) equipped with an Ultra1 column (50 m x 0.2 mm diameter, 0.33 µm

259 film thickness) was connected to a DeltaVPlus isotope ratio mass spectrometer through a modified GC-Isolink

260 interface. Each sample was separated chromatographically using~~with~~ a temperature program that started with an

261 oven temperature of 80 °C, which was held for 3 min, ramped to 250 °C with 3 °C per min and then ramped to

262 320 °C with 5 °C per min and finally reached temperature of 325 °C with a ramp of 1 °C per min and held for

263 15 min. The organic substances of the GC effluent stream were oxidized to CO_2 in the combustion furnace held at

264 940 °C on a CuO/Ni/Pt catalyst. Samples were measured in duplicate and the standard deviation was ≤0.5 ‰. The

265 quality of the isotope measurements was checked regularly (for each analysis) by measuring different *n*-alkane

266 standards with known isotopic composition of n-C15, n-C20, n-C25 (in equal concentration) and n-C16 to n-C30

267 (in various concentrations) ~~(~~ provided by Campro Scientific, Germany and Arndt Schimmelmann, Indiana

268 University, USA~~)~~.

269 GDGTs were re-dissolved in 120 µl hexane:isopropanol (v/v 99:1) and filtered through polytetrafluoroethylene

270 filters (0.45 µm in diameter) and analyzed using high performance liquid chromatography (HPLC, Agilent 1200

271 series HPLC system) coupled to a single quadrupole mass spectrometer (MS, Agilent 6120 MSD) *via* an

272 atmospheric pressure chemical ionization (APCI) interface. The individual GDGTs were separated at 30 °C on a

273 Prevail Cyano column (150 mm x 2.1 mm, 3µm). After injection of the sample (20 µl) it passed a 5 min isocratic

274 elution with mobile phase A (hexane/2-propanol/chloroform; 98:1:1, flow rate 0.2 ml/min). The mobile phase B

275   (hexane/2-propanol/chloroform; 89:10:1) was increased to 100% in two steps: a linear increase to 10% over 20

276   min followed by an increase to 100% within 10 min. During the measurement, the column was cleaned after 7 min

277   *via* backflush (5 min, flow 0.6 ml/min) and re-equilibrated with solvent A (10 min, flow 0.2 ml/min). The

278   conditions of the APCI were a nebulizer pressure of 50 psi, vaporizer temperature and N_2 drying gas temperature

279   350 °C, flow 5 l/min, capillary voltage 4 kV, and corona current 5 µA. Following Liu et al. (2020), iGDGTs and

280   brbranchedTthe GDGTs were detected by selective ion monitoring (SIM) of (M+H$^+$) ions (dwell time 76 ms) using

281   their molecular ions (GDGTs-1 (m/z 1300), GDGTs-2 (m/z 1298), GDGTs-3 (m/z 1296), crenarchaeol (m/z 1292)

282   and GDGTs-Ia (m/z 1022), GDGTs-IIa (m/z 1036), GDGTs-IIIa (m/z 1050)) and quantified. iIn relation to the

283   internal standard C_{46} (*m/z* 744). the molecular ions *m/z* of GDGTs-I (*m/z* 1300), GDGTs-II (*m/z* 1298), GDGTs-

284   III (*m/z* 1296), and crenarchaeol (*m/z* 1292) were quantified. Also, the branched GDGTs-Ia (*m/z* 1022), GDGTs-

285   IIa (*m/z* 1036), GDGTs-IIIa (*m/z* 1050) were quantified. The hydroxylated GDGTs OH-GDGT-0 (*m/z* 1318), OH-

286   GDGT-1 (*m/z* 1316), and OH-GDGT-2 (*m/z* 1314) were quantified in the scans of their related GDGTs (Fietz et

287   al., 2013). The standard deviation was 0.01 units of TEX^L_{86}.

288   Kalanetra et al. (2009) showed that GDGT-producing Thaumarchaeota are abundant in subsurface marine waters

289   in both Arctic and Antarctic regions. As Thaumarchaeota were found between 50 m and 200 m water depth in

290   Antarctica (Kim et al., 2012), temperatures based on GDGTs are suggested to reflect sub-surface waters

291   (Etourneau et al., 2013, 2019). Similarly, also RI-OH' based temperatures in Prydz Bay have been interpreted to

292   reflect subsurface water temperatures (Liu et al., 2020). We therefore consider our results to reflect subsurface

293   ocean temperatures (SOTs). We calculated TEX^L_{86} after Kim et al. (2012) with the *m/z* 12963 (GDGT-3), *m/z*

294   1298 (GDGT-2), *m/z* 1300 (GDGT-1):

295   $$TEX^L_{86} = \log \log \left(\frac{[GDGT-2]}{[GDGT-1]+[GDGT-2]+[GDGT-3]} \right)$$

296   (2)

297   and calibrated with SOT = 50.8 * TEX^L_{86} + 36.1 (Kim et al., 2012).   (3)

298   For the calculation of temperatures based on hydroxylated GDGTs we followed the approach of Lü et al. (2015)

299   $$RI - OH' = \frac{[OH-GDGT-1]+2\times[OH-GDGT-2]}{[OH-GDGT-0]+[OH-GDGT-1]+[OH-GDGT-2]}$$ (4)

300   and calibrated it with SOT = (RI-OH' - 0.1) / 0.0382.   (5)

301   For the branched and isoprenoid tetraether (BIT) index for indicating terrestrial organic matter (Hopmans et al.,

302   2004) we used crenarchaeol (m/z 1292) and the branched GDGTs and calculated it as:

303   $$BIT = \frac{[GDGT-Ia]+[GDGT-IIa]+[GDGT-IIIa]}{[Crenarchaeol]+[GDGT-Ia]+[GDGT-IIa]+[GDGT-IIIa]}.$$ (6)

304

2.4 Diatom analyses

We selected a set of 76 samples for the analysis of diatom assemblages. At first, sampling resolution was every 40-50 cm; thereafter, and based on the biogenic opal results, resolution was increased (every 8 cm) at intervals with high variability. ~~and then was increased~~ Freeze-dried samples (20-120 mg) were treated with hydrogen peroxide and sodium pyrophosphate to remove organic matter and clays, respectively, washed several times with DI water until reaching neutral pH. The treated samples were then settled for six hours in B-Ker2 settling chambers to promote an even distribution of settled particles (Scherer, 1994; Schrader and Gersonde, 1978; Warnock and Scherer, 2015). Once the samples were dry, the quantitative slides were mounted with Norland mounting medium (refraction index=1.56). Diatom valves per slide were counted across traverses (at least 400 valves per slide) using an Axioscop 2 Plus and Olympus BX60 at a magnification of ×1000. The counting procedure and definition of counting units followed those of Schrader and Gersonde (1978). We performed two sets of counts, with and without *Chaetoceros* resting spores. Diatoms were identified to species or species group level and, if applicable, to variety or form level following the taxonomy described by e.g., Gersonde and Zielinski (2000), Armand and Zielinski (2001), Esper et al. (2010), Esper and Gersonde (2014a, 2014b). Diatom ~~studies~~ analyses were done by the same investigator at the University of Concepción, Chile, and at Colgate University, USA.

Because diatom distribution in the Southern Ocean is directly associated with the temperature zonation and the frontal systems of the ACC (Cárdenas et al., 2019; Esper et al., 2010; Esper and Gersonde, 2014a, 2014b; Zielinski and Gersonde, 1997), diatom species were grouped into ecological assemblages reflecting i) seasonal sea ice – associated with temperatures -1.8 to 0°C; ii) cold open ocean – associated with the maximum sea-ice extent in winter and temperatures between 1 and 4°C; iii) warmer open ocean – with temperatures between 4 and 14°C, and iv) benthic-epiphytic habitats (Buffen et al., 2007; Cárdenas et al., 2019). Additionally, a group of reworked diatoms was identified (supplement section 6).~~Diatom species were grouped into ecological assemblages reflecting i) seasonal sea ice, ii) cold open ocean, iii) warmer open ocean, and iv) benthic-epiphytic diatoms environments (Buffen et al., 2007; Cárdenas et al., 2019; Esper et al., 2010)~~ (specific group composition is described in detail in supplement section 3). ~~Additionally, a group of reworked diatoms was identified.~~ A Spearman principal component analysis (PCA) was applied to the diatom assemblages to differentiate their temporal distribution.

For estimation of winter sea ice (WSI) concentrations, we applied the transfer function MAT-D274/28/4an to the total diatom counts (including Chaetoceros resting spores). The transfer function ~~which~~ comprises 274 reference samples with 28 diatom taxa/taxa groups and considers an average of 4 analogues (Esper and Gersonde, 2014a). The analogues refer to surface sediments from the Atlantic, Pacific and western Indian sector of the Southern Ocean. There are 10 analogues from the immediate vicinity of the Antarctic Peninsula. The WSI renders sea -ice

Formatiert: Englisch (Vereinigtes Königreich)

Formatiert: Englisch (Vereinigtes Königreich)

336 concentrations in a 1° by 1° grid for the September average of the period 1981 to 2010 (Reynolds et al., 2002,

337 2007). The threshold ~~of an~~between the open ocean and the~~to~~ sea ice covered area is set at 15% of sea ice

338 concentration (Zwally et al., 2002) and the average sea ice edge is defined at 40% (Gersonde et al., 2005; Gloersen

339 et al., 1993). ~~The qualitative estimation of sea ice concentration was derived from the abundance pattern of diatom~~

340 ~~sea-ice indicators (Gersonde and Zielinski, 2000).~~ The estimation of summer sea surface temperature (SSST) came

341 from the transfer function IKM-D336/29/3q comprising 336 reference samples (Pacific, Atlantic and Indian

342 Southern Ocean) with 29 diatom taxa and three factors (Esper and Gersonde, 2014b). The calculations for WSI

343 were done with the software R (R Core Team, 2012) using the packages Vegan (Oksanen et al., 2012) and

344 Analogue (Simpson and Oksanen, 2012).

345 **3   Results**

346 Based on our age model, ~~the~~ sediment core PS97/072-1 covers the last 13.89 ka BP with a mean sedimentation

347 rate of 67 cm/ka and a temporal resolution ranging between 50 and 150 years per sample interval. We note a higher

348 sedimentation rate of 95 cm/ka between 5.5 ka and 3 ka BP and few short-~~term~~ intervals of ~~significantly~~

349 ~~particularly~~ lower~~ed~~ (19 cm/ka) and higher~~enhanced~~ (190 cm/ka) sedimentation (Fig. 2).

350 Organic geochemical bulk parameters (TOC, biogenic opal), concentrations of HBIs ($IPSO_{25}$, $C_{25:3}$ HBI triene) and

351 diatom species of warm~~er~~ open ocean conditions ~~and sea ice~~ assemblages of piston core PS97/072-1 are

352 summarized in Figure 3 (additional data can be found in the supplement section 34). TOC increases from very low

353 values of 0.1 wt% at 13.7 ka BP to an average concentration of ~0.8 wt% between 9.9 ka BP and the top of the

354 core with recurring short-lived minima down to 0.03 wt% during the Middle and Late Holocene (Fig. 3f). Some

355 of these TOC minima ~~may be associated with~~occur within thin sandy layers of volcanic ash. Biogenic opal shows

356 a similar pattern with minimum values in the lower part of the record (3.2 wt% at 13.0 ka BP) and increases

357 throughout the Deglacial to Holocene with average values of 30 wt% and a maximum of 54.4 wt% at 5.3 ka BP

358 (Fig. 3e).

359 Between 13.89 ka and 13.4 ka BP, both $IPSO_{25}$ and HBI triene concentrations are close to or below the detection

360 limit (0.1 µg g^{-1}/g OC). Throughout the record, the~~The~~ $IPSO_{25}$ concentration ranges between 0.1 to 31.5 µg g^{-1}

361 TOC, while the concentration of the HBI triene ranges between 0.1 and 6.6 µg g^{-1} TOC (Fig. 3). $IPSO_{25}$ is absent

362 before 13.5 ka BP and rises rapidly to maximum values of 31.5 µg g^{-1} TOC at 12.89 ka BP. Subsequently,

363 concentrations decrease steadily until 8.5 ka BP and then remain at~~on~~ an average level of ~4 µg g^{-1} TOC with a

364 slightly decreasing trend to 1 µg g^{-1} TOC towards the present and smaller peaks of 10 µg g^{-1} TOC at 6.0 and 3.0

365 ka BP. Only traces of T~~t~~he HBI triene occur ~~at very low concentrations is largely absent~~ until 13.0 ka BP, while

366 its concentration ~~and~~ increases to ~~shows high~~ elevated concentrations up to 6.6 µg g^{-1} TOC after 8.5 ka BP with

367 large fluctuations of more than 5 µg g^{-1} TOC in the Middle Holocene and from 3.4 ka BP to the present.

368 The diatom composition has two contrasting groups indicating open ocean conditions, a cold water assemblage

369 and a warm~~er~~ water assemblage, and a seasonal sea ice assemblage (Fig. 3; see supplement section 3). ~~The diatom~~

370 ~~composition has two contrasting groups indicating warm~~ ~~open ocean conditions (Fig. 3a) and seasonal sea ice (Fig.~~

371 ~~3c).~~ Although the group reflecting seasonal sea ice is ~~also~~ present throughout the core (mostly >20%), the highest

372 contributions are seen before 1~~3~~2.8 ka BP and ~~,~~ between 10.8 and 9.9 ka BP ~~and around 3 ka BP~~. The contribution

373 of the warm~~er~~ open ocean assemblage is very low in the Deglacial and Early Holocene, ~~and~~ rises to highest values

374 in the Middle Holocene and remains around 10% in the Late Holocene. A biplot of a principal component analysis

375 (PCA) shows the relationship of the ecological groups ~~along the sediment core~~for three time intervals with clear

376 dominance of seasonal sea ice before 13.~~3~~ ka BP and warmer open ocean conditions after 8.5 ka BP (supplement

377 section 5 and 6~~4~~).

378 Sea ice concentration estimates based on diatom assemblages (WSI) and the PIPSO$_{25}$ index as well as the content

379 of IRD in PS97/0~~7~~2-1 are summarized in figure 4 (a-c). Reconstructed winter sea ice concentrations (% WSI)

380 derived from the MAT transfer function ~~results from the diatom assemblages~~ range from 80% to 90% during the

381 ACR and the Deglacial (13.8~~9~~ ka – 11 ka BP) and exhibit an overall decreasing trend over the Middle Holocene

382 with ~~distinct~~ fluctuations reaching minimum sea ice concentrations of ca. 65% during the Middle and Late

383 Holocene (Fig. 4a). PIPSO$_{25}$ values show a similar trend indicating higher sea ice cover during the ACR, the

384 Deglacial and the Early Holocene (PIPSO$_{25}$ > 0.8) and a successive decline to 0.5 on average throughout the

385 Middle and Late Holocene with a distinct minimum at 0.5 ka BP (Fig. 4b). IRD (lithic particles and pebbles > 5

386 µm) occurs frequently between 13.8~~9~~ ka and 9 ka BP and is virtually absent in the younger part of the sediment

387 core (Fig. 4c).

388 Figure 5 provides ocean temperature anomalies~~reconstructions~~ based on diatom assemblages (SSST) and GDGT-

389 derived RI-OH' and TEX$_{86}^{L}$ SOTs in core PS97/0~~7~~2-1 (Fig. 5 b-d). Diatom-derived SSST estimates ~~derived from~~

390 ~~diatom data~~ generally depict~~have~~ lower~~minimum~~ temperatures ~~of -1.5 °C to 0 °C~~ during the Deglacial and Early

391 Holocene, accompanied by ~~and~~ a shift to ca. 1 °C warm~~ing~~er temperatures ~~trend (to > 0 °C)~~ in the Middle and

392 Late Holocene ~~with a distinct cold event at 3.1 ka BP~~ (Fig. 5b). A short cold event with a SSST decrease of ca. 1.5

393 °C occurred a~~t~~round 3.1 ka BP. Similar to SSSTs, ~~also~~ RI-OH'-derived SOTs likewise reflect generally lower

394 temperatures during the Deglacial and Early Holocene, and ~~between -1.9 to -1.2 °C and~~ a similar trend of rising

395 0.4 °C warmer temperatures in the Middle and Late Holocene ~~to -1.2 °C until 4.2 ka BP followed by a subtle~~

396 ~~cooling to -1.4 °C~~ (Fig. 5c). TEX$_{86}^{L}$-derived SOTs ~~data from GDGTs cover a temperature range of 0.7 to 3.8 °C~~

397 ~~and~~ display an opposite trend to both SSST and RI-OH' SOT with peak temperatures ~~decreasing temperatures to~~
398 ~~0.7 °C since~~ ~~from~~ during the Deglacial and an overall Holocene cooling towards present (Fig. 5~~e~~d).

399

4   Discussion

4.1 The late Deglacial (13.8~~14~~ ka to 11.7 ka BP)

402 In the oldest part of our sediment record, covering the later part of the last Deglacial from 13.8~~14~~ ka until 11.7 ka
403 BP, we observe a remarkable environmental change indicated by ~~significant~~ large shifts in the TOC, biomarker
404 and diatom records (Fig. 3). T~~Before 13.4 ka BP, t~~he very low concentrations of HBIs~~biomarkers~~ (Fig. 3b and d),
405 TOC (Fig. 3f), and biogenic opal (Fig. 3e) between 13.8 ka and 13.5 ka BP suggest that primary production of
406 phytoplankton ~~associated with open marine conditions~~ and also sea ice algae synthesizing IPSO$_{25}$~~settings~~ was

407 diminished, while sea -ice related diatom species show the highest contribution of 73% (Fig. 3c), albeit with very
408 low concentrations (~~supplement section~~ see online ressource5). Highest WSI concentrations ~~values of winter sea~~
409 ~~ice Highest~~ (WSI, Fig. 4a) and PIPSO25 values ~~spring sea ice (PIPSO$_{25}$, Fig. 4a, b) indicators and WSI values~~ are
410 pointing towards a maximum sea ice cover ~~that lasted until summer~~in both seasons and are. ~~Lowest and lowest~~
411 ~~ocean temperatures reflected in the RI-OH' derived SOTs are~~ well in line with peak ssNa concentrations ~~and~~
412 ~~minimum δ^{18}O values~~ in the EDML and, WAIS ~~and JRI~~ ice core records, referring to an extended sea ice cover
413 until 13 ka BP ~~and lowered atmospheric temperatures~~ (Fig. 4; EPICA Community Members, 2006; Fischer et al.,
414 2007; WAIS Divide Project Members, 2015). We note that for the interpretation of PIPSO$_{25}$ values, changes in

415 both IPSO$_{25}$ and HBI triene concentrations need to be evaluated carefully to reliably deduce information on sea

416 ice conditions. High PIPSO$_{25}$ values may refer to an extended sea ice cover that lasts until summer (thus hampering

417 phytoplankton productivity/HBI triene synthesis), whereas low PIPSO$_{25}$ values point to a reduced sea ice cover in

418 terms of duration (in spring) and/or sea ice concentration. ~~TIn agreement with the biogenic opal and t~~The near
419 absence of IPSO$_{25}$, the HBI triene ~~and~~ and warm open ocean diatom species ~~as well as minimum contents in TOC~~
420 ~~and biogenic opal~~ between 13.8~~9~~ ka and 13.5 ka BP evidences a ~~very thick or~~ permanent, potentially perennial ~~sea~~
421 ice cover or at least sea ice that wa~~si~~s too thick to allow photosynthesis of sea ice algae inhabiting ~~at~~ the sea ice
422 ~~bottom~~. Similarly, Lamping et al. (2020) relate~~d~~ the absence of IPSO$_{25}$ and ~~a~~ phytoplankton-derived dinosterol
423 ~~biomarker~~ in sediments in the western Amundsen Sea to the re-advance of a floating ice shelf canopy during the
424 ACR. At the PS97/072-1 core site in the eastern Bransfield Strait, both the presence of perennial sea ice, or an ice
425 shelf tongue extending from the APIS, could explain the lack of indicators of phytoplankton productivity and
426 IPSO$_{25}$-synthesizing ice algae. We hence assume that the very low absolute concentrations of sea ice -associated

427 diatoms result from lateral transport underneath the ice or reworking of sediments older than 13.5 ka BP. TtThe

428 abrupt increase in IPSO$_{25}$ concentrations at 13.5 ka BP, however, may indicate the retreat or thinning of such an

429 ice-shelf covercanopy, from the core site permitting sea ice algae growth during spring and a subsequent increase

430 in primary production reflected in rapidly rising HBI triene concentrations sinceat 13 ka BP (Fig. 3b, d). Such a

431 transition from a perennial floating ice canopy to conditions characterized by (seasonal) sea ice cover is also

432 reported by Milliken et al. (2009)for the nearby Maxwell Bay (King George Island; SSI) between 14 ka and 10 ka

433 BP. Interestingly, Aa significant prominent decrease in sea ice associated diatoms between 13 ka and 12 ka BP

434 (Fig. 3c), however, is not mirrored by the still high WSI concentrations. This discrepancy could relate to a weaker

435 preservation potential of certain diatoms reflecting seasonal sea ice (e.g. Synedropsis sp., Nitzschia stellata) that

436 are not considered within the transfer function to estimate WSI, which highlights the need to examine silica

437 dissolution effects for the interpretation of diatom records. We note that traces of biomarkers and diatoms

438 (supplement section 4 and 65) deposited in sediments older than 13.5 ka BP may reflect sub-ice shelf lateral

439 advection and reworking (Smith et al., 2019).

440 With regard to the ocean temperatures recorded at core site PS97/072-1, we note that the overall cool deglacial

441 temperatures derived from diatom data (SSST) and hydroxylated GDGTs (RI-OH') seem to be linked to the

442 lowered summer insolation (Fig. 5a), whereas higher TEX$_{86}^L$ temperatures seem to be associated with a higher

443 spring insolation (Fig. 5d). While the impact of seasonality on GDGT-based ocean temperature estimates is still

444 under debate and would require further improvements in on regional calibration, the observation of maximum

445 abundances of thaumarchaeota species (producing isoGDGTs applied to determine TEX$_{86}^L$) in Antarctic coastal

446 waters during spring (Kalanetra et al., 2009; Murray et al., 1998) seems to support our interpretation and also helps

447 to explain the divergent trends in TEX$_{86}^L$ and RI-OH' derived SOT estimates, as the latter proxy might be also

448 sourced by other archaea species that probably grow mostly during the summer season.

449 While the ACR lasts from 14.7 ka to 13 ka BP (Pedro et al., 2016) as indicated by e.g. the WAIS Divide ice core

450 records from JRI (Fig. 5h, Mulvaney et al., 2012) and WAIS Divide (Fig. 5i, WAIS Divide Project Members,

451 2013), our sediment record shows that cold conditions with an extended sea ice cover, limiting summer

452 phytoplankton productivity (Fig. 4a, b) and reduced summer ocean temperatures in the eastern Bransfield Strait,

453 lasted until ca. 11 ka BP (Figs. 4 and 5). Further, the Deglacial and Early Holocene (Fig. 4c) IRD content (Fig.

454 4.c; including the presence of single large pebbles) in core PS97/072-1 points to the frequent occurrence of

455 icebergs, during the Deglacial and the Early Holocene (Fig. 4c), which relates related toevidencing the overall ice

456 sheet disintegration alongt the WAP that occurred around 14 ka BP at the SSISouth Shetland Islands and promoted

457 seasonally open-marine conditions at Anvers-Hugo Trough at 13.6 ka BP (middle WAP shelf) and and at 123.92

ka BP inat Palmer Deep at the southern (inner WAP shelf), respectivelyAP (Domack et al., 2001; Domack, 2002; Jones et al., 2022; Milliken et al., 2009; Roseby et al., 2022). At our core site, rising RI-OH' SOTsA and a slight decrease in PIPSO$_{25}$ values and rising RI-OH' SOTs characterize the late Deglacial between 13 ka and 11.7 ka BP (Fig. 4b, 5c). A prominent decline in large-scale sea ice cover is also reflected in the decreasing ssNA concentrations in the EDML and WAIS ice cores between 13 ka and 11.7 ka BP (Fig. 4e, f) and is likely related to a distinct atmospheric warming, as reflected in ice core stable water isotopes (Fig. 5h).

The ACR cooling and the subsequent Late Deglacial This subsurface ocean warming may relate to inter-hemispheric teleconnections through a global reorganization of atmospheric and ocean circulation that is associated withrelated to the bipolar seesaw pattern of opposite climate trends between the northern and southern hemisphere (Anderson et al., 2009; Broecker, 1998; EPICA Community Members, 2006; Pedro et al., 2016). While a northward shift of the southern westerlies during the ACR (Fletcher et al., 2021) promoted Antarctic sea ice expansion and glacier readvance (potentially affectingcausing an ice cover over the PS97/072-1 core site), ... a With cooling of the northern hemisphere andwith, a southward shift of the Intertropical Convergence Zone and the southern hemisphere westerlies (Lamy et al., 2007) resulted in intensified wind stress in the Drake Passage (Timmermann et al., 2007). and This pattern would have increased upwelling that may have driven the continued ocean warming and sea ice retreat in Antarctica towards the Holocene (Anderson et al., 2009).

4.2 Early Holocene warming from 11.7 ka to 8.2 ka BP

The Early Holocene from 11.7 ka to 8.2 ka BP is characterized by a progressively decreasing spring sea ice cover inferred from shown by declining PIPSO$_{25}$ values (Fig. 4b), as well asthough highly variable winter and spring sea ice cover with prominent as shown by further declining WSI shifts in sea ice concentration (from 90% to 65%; and PIPSO$_{25}$ values (Fig. 4a and b). These WSI fluctuations are not reflected in the sea ice diatom assemblage, which, similar to the biogenic opal content, follows an increasing trend until 10.5 ka BP (Fig. 3c, e). Increased Improved accumulation of biogenic opal and a better preservation of (thin-walled) sea-ice-related diatoms that are not used for the transfer function may explain the mismatch between the WSI record and sea ice diatom assemblage. The increase in While biogenic opal is further accompanied by a risingand TOC contents exhibit increasing trends, while concentrations of the HBI triene and warm open ocean diatoms remain low and, only an significant increase after 9 ka BP, signalssignallingsuggests higher phytoplankton productivity (Fig. 3a, b). Diatom-derived SSSTs exhibit marked fluctuations but remain relatively low until 8.2 ka BP (Fig. 5b). RI-OH' and TEX$_{86}^{L}$ SOTs display diverging trends following the summer and spring insolation, respectively (Fig. 5).

488 ~~Ocean~~ temperatures ~~based on~~ warming is indicated by RI-OH' based SOT, while TEX_{86}^{L} SOT and diatom-derived

489 ~~SSST show fluctuating temperatures without a clear trend (Fig. 5b, c and d).~~

490 While $PIPSO_{25}$ values display a ~~rather~~ gradual decrease in sea ice coverage, the WSI record suggests a highly

491 variable sea ice cover, with several~~few~~ distinct sea ice minima between 11 ka and 10 ka BP and around 9 ka BP

492 (Fig. 4a and b). These sea ice minima may have resulted from punctuated warming events, *e.g.* a~~round~~t 10 ka BP,

493 when SSST shows a short temperature peak, which might have led to a delayed sea ice formation in autumn and

494 winter (Fig. 5b). Another WSI minimum at 9 ka BP coincides with a major, final ~~(and final)~~ peak in IRD deposition

495 at the core site (Fig. 4), evidencing iceberg discharge during episodes of peak AP ice-sheet ~~loss~~ retreat and

496 enhanced calving at the WAP (Jones et al., 2022). As sea ice melting may have been an important driver of ~~the~~

497 ocean stratification, we suggest warmer, stratified surface waters with moderate production in summer, supported

498 by increasing summer insolation ~~in December~~ (Fig. 5a). Ameliorating climate conditions, ice-shelf retreat along

499 the NAP and the establishment of modern-like ocean conditions after 9 ka BP have also been proposed for the

500 western Bransfield Strait ~~by (~~Heroy et al. (2008) and are well in line with the rising concentrations ~~contribution~~ of

501 warm open ocean diatoms and the phytoplankton-derived HBI triene at our core site after 9 ka BP (Fig. 3). The

502 general decrease in spring sea ice cover (reflected in declining $PIPSO_{25}$ values)~~Our marine records of decreasing~~

503 ~~sea ice~~ may have been fostered by~~and~~ a maximum spring and rising summer insolation (Fig. 5a, d), ~~and subsurface~~

504 ~~ocean temperatures~~ shortening the duration of sea ice cover. Rising RI-OH' temperatures ~~are which are~~ consistent

505 with the overall slight warming trend recorded in the WAIS Divide ice core (Fig. 5h), which has been shown to

506 be mainly driven by increasing summer temperatures (Jones et al., 2022). ..... ~~Interestingly, neither this rise in RI-~~

507 ~~OH' derived SOTs nor the highly variable~~ The decreasing TEX_{86}^{L} SOT~~temperature~~ trends at core site PS97/072-

508 1 corresponds to the declining TEX_{86} temperatures reported for ODP site 1098 ~~i~~at Palmer Deep (Fig. 5g;

509 Shevenell et al., 2011) though the latter displays a more pronounced temperature drop (of ca. 6 °C) between 11.7

510 ka and 8.2 ka BP.~~or the declining δD values recorded in the JRI ice core (Fig. 5; Mulvaney et al., 2012).~~ These

511 regional differences may relate to changing ocean circulation patterns, ~~and~~ associated shifts in water mass

512 distribution a~~long~~t the WAP ~~and EAP~~ and the local post-glacial environmental development during the Early

513 Holocene. Deposition of laminated diatom oozes in the Anvers-Hugo Trough at the WAP middle shelf during the

514 early Holocene ~~since 11.5 ka BP~~, *for example*~~e.g.~~, documents episodes of extremely high productivity in response

515 to a southward shift of the southern hemisphere westerlies and the advection of warm and nutrient-rich CDW

516 (Roseby et al., 2022). We propose that the eastern Bransfield Strait remained mainly "inaccessible" for CDW and

517 BSW until further ice recession between 10 ka and 5 ka BP (Ó Cofaigh et al., 2014 and references therein)

518 permitted advection of these water masses into the Bransfield Strait. ~~We further note that the partly opposing trends~~

519 ~~in RI-OH' and TEX$_{86}$^{L} temperatures at our core site could indicate that the respective GDGT producing archaea~~

520 ~~thrive in different water depths or during different seasons.~~

521

522 **4.3 Middle Holocene from 8.2 ka until 4.2 ka BP**

523 The Middle Holocene from 8.2 ka to 4.2 ka BP was~~is~~ a period of ~~significant~~ remarkable sea ice retreat and

524 minimum iceberg ~~flux~~ activity~~records~~ at the core site indicated by decreasing WSI and PIPSO$_{25}$ values and~~,~~

525 virtually absent IRD (Fig. 4)~~, and an oceanic warming reflected in SSST and RI-OH' SOT (Fig. 4 and 5)~~. D~~For~~

526 ~~the whole period, d~~iatoms associated with warmer open ocean conditions, peak HBI triene concentrations and

527 maximum TOC ~~and~~ as well as biogenic opal contents (Fig. 3) indicate~~refer to~~ a high export production during the

528 Middle Holocene ~~(Abelmann et al., 2006; Smetacek et al., 2004)~~. Th~~is~~e higher primary productivity~~export~~

529 ~~productivity~~production~~is~~ can be linked to a decrease in~~of~~ both winter and spring sea ice ~~and potentially ice-free~~

530 ~~summers~~ indicated by WSI and PIPSO$_{25}$ minima, respectively (Fig. 4a, b)~~, and~~ elevated SSSTs and (summer)

531 SOTs (Fig. 5b, c) promoting ice-free summer ocean conditions favorable for phytoplankton productivity. These

532 Middle Holocene sea–ice conditions compare well with ~~the~~ modern situation at the core site characterized by a

533 seasonal decrease in sea ice concentration from 50% during winter to mainly ice-free summers (NSIDC; Cavalieri

534 et al., 1996). ~~like it was observed for modern sea ice conditions in this region (Vorrath et al., 2020).~~.

535 The continued retreat of the previously grounded APIS~~AP ice sheet~~ adjacent to~~over~~ the Bransfield Strait between

536 10 ka and 5 ka BP finally opened the passage for ACC ~~surface~~ waters to enter the Bransfield Strait from the west

537 (Bentley et al., 2014; Ó Cofaigh et al., 2014). As a result, we suggest that sea ice conditions at our core site were

538 ~~predominantly~~ influenced by ~~branches~~ incursions of warmer ocean~~ic~~ waters carried~~associated with~~of the ACC

539 (i.e.~~the~~ BSW and CDW) ~~leading to a shorter sea ice season and/or less intensive sea ice cover~~, while~~and~~ cold water

540 inflow and sea ice advection from the Weddell Sea was diminished due to the still grounded ice sheet at the tip of

541 the AP (Ó Cofaigh et al., 2014), leading to a shorter sea ice season in the eastern Bransfield Strait. This shift

542 towards a warmer, less ice-covered ocean setting in the eastern Bransfield Strait is ~~well in line with~~reflected in the

543 transition from proximal to distal glacimarine conditions in Maxwell Bay (Milliken et al., 2009) and may be

544 associated with the Mid-Holocene climatic optimum. This timing contrasts the not~~a~~tion of Heroy et al. (2008),

545 who, ~~based on diatom assemblage analyses of a sediment core in the western Bransfield Strait,~~ confined~~s~~ the Mid-

546 Holocene climatic optimum to a shorter time interval between 6.8 ka and 5.9 ka BP based on diatom assemblage

547 analyses of a sediment core in the western Bransfield Strait. We propose that this temporal offset may relate to

548 regionally different responses, ~~to~~ glacial retreat patterns impacting oceanic pathways and the position of frontal

549 systems controlling primary productivity within ~~the~~ Bransfield Strait. The generally decreasing WSI and variable

550 PIPSO$_{25}$ values further depict different trends than PIPSO$_{25}$ values determined for the JPC10 in Palmer Deep (

551 Fig. 4d; Etourneau et al., 2013), which suggest an overall increase in spring sea ice along the WAP until 4.2 ka

552 BP. Though minima in spring sea ice at 7.5 ka, 6.5 ka and 5.4 ka BP at core site PS97/072-1 may be related

553 compare to PIPSO$_{25}$ minima observed for JPC10, the lack of Middle Holocene age constraintstie points in our core

554 from the Bransfield Strait detersprevents us from concluding on a common driver causingfor these sea ice

555 reductions. minima in spring sea ice at 6.5 ka and 5.4 ka BP The weak influence from the Weddell Sea limited the

556 export of cold waters and supported was weak and opposite sea ice conditions were reconstructed for in the eastern

557 AP where HBI biomarker and diatom assemblages record regionally extended sea ice cover between 7 ka and 4.5

558 ka BP (Fig. 4c, Barbara et al., 2016a; Minzoni et al., 2015).

559 Regarding ocean temperatures, we observe a sustained warming in RI-OH' SOT, punctuated by a cooling at 5.5

560 ka BP (Fig. 5c), while TEX$_{86}^{L}$ temperatures depict a subtle cooling of ca. 0.5 to 0.9 °C between 8.2 ka and 7 ka

561 BP, followed by a warm reversal of up to 3.1 °C until 6 ka BP, and a further cooling until 4.2 ka BP (Fig. 5e).

562 ThisA Middle Holocene slight cooling trend is alsohas also been observed in the TEX$_{86}^{L}$ recordsat from the core

563 sites core sites at in Palmer Deep at the WAP (Fig. 1 and 5f, g;, Etourneau et al., 2013; Shevenell et al., 2011).

564 The similarity between these records encourages us to assume that these TEX$_{86}$-derived temperatures from along

565 the WAP and NAP are driven by spring insolation rather than reflectingbeing a reflection of annual mean ocean

566 temperature conditions (see above). and contrasts a rapid warming observed in JPC38 from the eastern AP

567 between 8 ka and 6.5 ka BP (Fig. 1 and 5, Barbara et al., 2016; Etourneau et al., 2019). Here, the near coastal

568 marine sediment core close to JRI (Fig. 5g, Barbara et al., 2016) records the transition from cold and heavily sea

569 ice covered conditions at 8.2 ka BP to a warmer water environment with reduced sea ice cover permitting more

570 phytoplankton growth between 6.5 ka and 4.2 ka BP (Barbara et al., 2016). Since stable temperatures are inferred

571 from the JRI ice core during the entire Middle Holocene (Mulvaney et al., 2012), we suggest that the environmental

572 changes recorded in JPC38 reflect ocean driven rather than atmospheric processes.

573

574 **4.4 Late Holocene and Neoglacial from 4.2 ka BP until today**

575 The Late Holocene covering the past 4.2 ka BP is characterized by a highly variable winter sea ice and decreasing

576 spring sea ice cover at core site PS97/072-1, as indicated reflected in the MAT-derived WSI and a decline in

577 PIPSO$_{25}$ values over the past 2 ka (Fig. 4a, b). Rather constant relatively stable environmental conditions at our

578 core site reflected in constant biogenic opal and TOC contents (Fig. 3e, f), however, suggest that primary

579 productivity remained relatively unaffected by this reduction in spring sea ice cover. low While decreasing IPSO$_{25}$

580 concentrations between 2.5 ka BP and the core top (Fig. 3d) suggest a reduced productivity of the sea ice diatom

581 species synthesizing this molecule, no significant changes are observed in the sea ice diatom assemblage (Fig. 3c),

582 which supports the assumption that only a restricted group of diatoms - at least *Berkeleya adeliensis* - produce

583 $IPSO_{25}$ (Belt et al., 2016). The warm open ocean diatom assemblage follows an overall declining trend throughout

584 the Late Holocene, which is not reflected in the highly variable and slightly increasing HBI triene concentrations

585 (Fig. 3a, b), and a prominent decrease in HBI triene concentrations occurs only at 1 ka BP. which display a slight

586 increase until it decline and still variable but elevated HBI triene concentrations. A gradual decline in $PIPSO_{25}$

587 values between 4.2 ka and 1.5 ka BP contrasts the highly variable WSI concentrations (Fig. 4). …While the

588 observation of cooler sea surface temperatures, and a diminished spring sea ice cover indicated by the joint

589 decrease in the warm open ocean diatom assemblage and $PIPSO_{25}$ values since 2 ka BP may seem counterintuitive,

590 Milliken et al. (2009) report a similar development in Maxwell Bay since 2.6 ka BP. Interestingly, records of

591 diatom and radiolarian assemblages of a sediment core (Gebra-2) collected in very close vicinity to PS97/072-1

592 document an overall increase in sea-ice taxa over the past 3 ka BP with distinct Neoglacial events characterized

593 by higher (denser and longer) sea ice cover (Bárcena et al., 1998). The lower sampling resolution and missing age

594 control for the past 3 ka BP in PS97/072-1, however, hamper a more detailed comparison of diatom species in our

595 core with those investigated for Gebra-2. The Neoglacial increase in (spring) sea ice cover is also indicated by a

596 prominent rise of $PIPSO_{25}$ values determined for JPC10 in Palmer Deep (Fig. 4d; Etourneau et al., 2013).

597 Similarly, deposition of ssNa in the EDML ice core (Fischer et al., 2007) increases since 2 ka BP.

598 Minimum PS97/072-1 $PIPSO_{25}$ values at 0.5 ka BP result fromare duerelated to the significantly notably reduced

599 $IPSO_{25}$ and HBI triene concentrations (Fig. 3b, d). While Similar to our observation for the Deglacial, this pattern

600 of minimumlow HBI triene and minimum lowest $IPSO_{25}$ concentrations is similar to the period between 13.8 ka

601 and 13.5 ka BP, which was characterized by , may point to perennial cold conditions and a heavypronounced -

602 potentially perennial - ice cover, the elevated TOC and biogenic opal values, as well as the presence of diatoms

603 associated with warm open ocean conditions at 0.5 ka BP, point to favorable ocean conditions. We hence relate

604 this drop in HBI concentrations to a shift in the diatom community rather than to an abrupt readvance of an ice

605 cover.

606 Late Holocene ocean temperature reconstructions for core PS97/072-1 display different patterns. Generally

607 increasing diatom-derived SSSTs are only punctuated by a cooling event at 3.1 ka BP, while RI-OH' SOT remains

608 relatively constant with a very subtle cooling of ca. 0.2 °C between 1.5 ka and the present, which could be linked

609 to the slight decrease in summer insolation (Fig. 5a, b, c). The decrease in TEX_{86}^{L} SOT by about 1 °C between 4

610 ka and 3.3 ka BP in eastern Bransfield Strait is also depicted in the TEX_{86}^{L} data from the Palmer Deep core JPC10

611 (Fig. 5e, f; Etourneau et al., 2013). The following warming reflected in PS97/072-1 TEX_{86}^{L} SOT until ca. 2 ka

612 BP may relate to the establishment of open marine conditions fostering primary productivity at the Perseverance

613 Drift north of Joinville Island (northern tip of the AP) as a result of warm water intrusions (Kyrmanidou et al.,

614 2018). This warming is reversed by another cooling at about 2 ka BP - coincident with an abrupt temperature

615 increase of ca. 4 -°C depicted in the ODP1089 TEX$_{86}$ SOT record in Palmer Deep (-Fig. 5g; Shevenell et al., 2011).

616 The latter~~This~~ warming is not displayed in the TEX$_{86}^{L}$ data of the nearby JPC10 and we relate this contrast to the

617 different approaches used to determine SOT (*i.e.*, TEX$_{86}$ vs. TEX$_{86}^{L}$ omitting the crenarchaeol regio-isomer, which

618 seems to be less important for membrane adaptation in polar waters; Kim et al., 2010).

619 Evidently, temperature trends at the AP in the Late Holocene are highly variable between different areas (Allen et

620 al., 2010; Barbara et al., 2016; Bárcena et al., 1998; Bentley et al., 2009; Etourneau et al., 2013; Mulvaney et al.,

621 2012; Shevenell et al., 2011) and this is likely associated with the complex oceanographic and atmospheric

622 settings. This heterogeneous pattern, however, contrasts ~~with~~ the currently observed large-scale ocean warming

623 along the AP driven by intrusions of ACC-derived warm CDW onto the continental shelf of the WAP (Couto et

624 al., 2017) and the NAP (Ruiz Barlett et al., 2018), as well as the overall loss of sea ice (Parkinson and Cavalieri,

625 2012), which supports the assumption that the changes impacting the AP already exceed natural variability.

626 ~~conditions and the establishment of thick and/or compacted sea ice limiting the productivity of both phytoplankton~~

627 ~~and also sea ice diatoms. This short period of sea ice growth may be related to the Little Ice Age (LIA), when~~

628 ~~cooler conditions also triggered glacial readvance at the Antarctic Peninsula 500 years ago (*e.g.* Simms et al.,~~

629 ~~2021). While a significant large~~ pulse in sea ice export from the Arctic Ocean is proposed to have caused the LIA

630 ~~cooling (Miles et al., 2020), knowledge about LIA sea ice conditions in the Southern Ocean is scarce and hence~~

631 ~~inconclusive (Parkinson, 1990). The~~ Neoglacial cooling as found in the JRI ice core, for example, is clearly

632 ~~reflected in an increased sea ice cover at Palmer Deep since 2 ka BP (Fig. 4d, Etourneau et al., 2013) but this~~

633 ~~record, however, contains no clear evidence for a further expansion of sea ice in response to the LIA. We conclude~~

634 ~~that a comprehensive assessment of how Antarctic sea ice conditions changed during the LIA requires more studies~~

635 ~~of well-dated and ideally higher resolved sediment records.~~

636 ~~Similar to our sea ice signals, also the Late Holocene ocean temperature reconstructions display different patterns.~~

637 ~~While RI-OH' SOT remains relatively stable, TEX$_{86}^{L}$ indicates a cooling around 3 ka BP followed by a warming~~

638 ~~until 1.5 ka BP and another cooling towards the top of the core. Diatom-derived SSST also point to a cold period~~

639 ~~around 3 ka BP immediately followed by peak~~a warming peak at ca. 2.5 ka BP. Evidently, temperature trends at

640 ~~the WAP in the Late Holocene are highly variable between different areas (Allen et al., 2010; Barbara et al., 2016;~~

641 ~~Bárcena et al., 1998; Bentley et al., 2009; Etourneau et al., 2013; Mulvaney et al., 2012; Shevenell et al., 2011)~~

642 ~~and this may relate to the complex oceanographic and atmospheric settings. With regard to the diverging~~

5   Conclusions

648 We reconstruct~~eded~~ the sea ice and climate development at the N~~northwest~~ AP since the last Deglacial using the

649 sediment core PS97/072-1 from the eastern Bransfield Strait. Pursuing a multi-proxy approach that focuses on

650 organic geochemical bulk and biomarker analyses, diatom assemblage studies and transfer functions as well as

651 IRD data, we identifie~~dy~~ different Deglacial and Holocene environmental conditions impacted by sea ice and

652 ocean temperature changes.~~. In our multiproxy study we focused on the sea ice biomarker IPSO₂₅, the HBI z-triene~~

653 ~~representing open marine environments, and GDGTs for ocean temperature reconstructions. Diatom ecological~~

654 ~~groups characteristic of sea ice or~~ ~~cold/ warmer~~ ~~open ocean conditions were used, as well as diatom transfer~~

655 ~~functions to reconstruct winter sea ice and summer sea surface temperature. Additional information was derived~~

656 ~~from sedimentological records such as IRD~~ ~~and biogenic opal.~~ Our results reveal the retreat of a perennial ice

657 cover~~floating ice shelf canopy~~ after the ACR and an overall sea ice reduction~~retreat~~ and ~~summer ocean~~ warming

658 summer ocean temperatures during the Holocene. The late Deglacial from 13.8~~9~~ ka to 11.7 ka BP was a highly

659 dynamic period: until 13.4 ka BP primary productivity~~the sedimentation of organic proxies~~ was diminished due to

660 a permanent ice cover during the ACR. The ACR terminated with a shift to slightly warm~~ing~~ conditions at 13 ka

661 BP along with a reduction~~retreat~~ in the length of the ~~spring~~ sea ice season, which permitted phytoplankton

662 productivity at least during summer. The Early Holocene from 11.7 ka to 8.2 ka BP was characterized by increasing

663 summer ocean temperatures~~warming~~, further~~slightly~~ decreasing ~~(in terms of duration and/or sea ice concentration)~~

664 ~~spring~~ sea ice cover in terms of duration and/or sea ice concentration and highly variable winter sea ice cover. In

665 the Middle Holocene from 8.2 ka to 4.2 ka BP, increased advection of BSW and CDW led to a shortened sea ice

666 season (confined to winter and spring)~~ea ice coverage confined to winter and spring season~~ ~~stable environmental~~

667 ~~conditions prevailed with~~ ~~elevated~~ ~~and rising summer ocean temperatures fostering~~ primary production,

668 indicating ~~and this period may be associated with~~ the Middle Holocene Climatic Optimum ~~due to intervals of~~

669 ~~lower sea ice cover. In general, sea ice seasons were short and sea ice cover was significantly~~ greatly reduced to a

670 minimum around 5.5 ka BP, ~~even though high seasonal amplitudes and short-term, centennial changes in sea ice~~

671 ~~conditions occurred.~~ During the Late Holocene, the core site experienced ~~a~~ distinct fluctuations in~~variable~~ WSI

672 with concentrations shifting between 90% and 60%~~concentration,~~ ~~while~~ while PIPSO₂₅ values declined

673 continuously suggesting a less intensive or shorter spring sea ice cover~~spring sea ice declined continuously~~. ~~and~~

674 ~~a short-term SSST cooling at 3 ka BP. Phytoplankton biomarkers as well as sea ice proxies (IPSO$_{25}$, PIPSO$_{25}$,~~

675 ~~WSI) were lowest during the period coincident with the Little Ice Age which we relate to the establishment of a~~

676 ~~multi-year sea ice cover.~~ We note that GDGT-based TEX$_{86}^{L}$ and RI-OH' SOTs correspond to spring and summer

677 insolation, respectively, which may explain the divergent trends displayed by both SOT proxies. Clearly, while

678 this observation may help with the interpretation of other Southern Ocean GDGT-based temperature estimates and

679 the reconstruction of seasonal SOT variability, more investigations into the mechanisms driving GDGT synthesis

680 in polar waters are~~is~~ needed.

681

Data Availability

All data mentioned in this paper will be available at the open access repository www.pangaea.de (https://doi.pangaea.de/10.1594/PANGAEA.952279).

Author contributions

The study was conceived by MV and JM. Data collections and experimental investigations were done by MV together with CBL (core description, sampling, diatoms, biogenic opal, age model), PC (diatoms), AL (age model, diatoms), OE (diatom transfer function), GM (GDGTs ~~PS97/072-1~~, ^{14}C dating), AVH (δ^{13}C IPSO[25]), NL (δ^{13}C TOC), LLJ (foraminifera, age model), SMS (age model, humming age), ~~CBL (core description, sampling, diatoms, biogenic opal, age model), PC (diatoms), AL (age model, diatoms), OE (diatom transfer function), GM (GDGTs PS97/072-1, ^{14}C dating), AVH (δ^{13}C IPSO[25]), NL (δ^{13}C TOC),~~ J~~E~~e, DE and CE provided temperature and salinity profiles near the study site. MV drafted the manuscript. All authors contributed to the interpretation and discussion of the data and the finalization of this manuscript.

Competing interests

None of the authors have a conflict of interest.

Acknowledgement

We thank the captain, crew and chief scientist Frank Lamy of RV Polarstern cruise PS97. Denise Diekstall, Jens Hefter, Alejandro Avila and Victor Acuña are thanked for their laboratory support. We thank Helge Arz for his help with the age model. Simon Belt is acknowledged for providing the 7-HND internal standard for HBI quantification. Financial support was provided through the Helmholtz Research grant VH-NG-1101. Partial support from the Centers IDEAL (grant FONDAP 15150003) and COPAS ~~Sur Austral~~ (grants AFB170006 and FB210021), Chile, and the Spanish Ministry of Economy, Industry and Competitivity grants CTM2017-89711-C2-½-P, co-funded by the European Union through FEDER funds, is acknowledged. We appreciate~~acknowledge~~ support by the Open Access Publication Funds of Alfred-Wegener-Institut Helmholtz-Zentrum für Polar- und Meeresforschung.

712
713
714
715
716
717
718

References

719

720 Abelmann, A., Gersonde, R., Cortese, G., Kuhn, G. and Smetacek, V.: Extensive phytoplankton blooms in the

721 Atlantic sector of the glacial Southern Ocean, Paleoceanography, 21(1), 1–9, doi:10.1029/2005PA001199, 2006.

722 Alexander, V. and Niebauer, H. .: Oceanography of the eastern Bering Sea ice-edge zone in spring, Limn, 26(6),

723 1111–1125 [online] Available from: http://doi.wiley.com/10.1029/2007RG000250, 1981.

724 Allen, C. S., Oakes-Fretwell, L., Anderson, J. B. and Hodgson, D. A.: A record of Holocene glacial and

725 oceanographic variability in Neny Fjord, Antarctic Peninsula, The Holocene, 20(4), 551–564,

726 doi:10.1177/0959683609356581, 2010.

727 Allison, I., Tivendale, C. M., Akerman, G. J., Tann, J. M. and Wills, R. H.: Seasonal Variations In The Surface

728 Energy Exchanges Over Antarctic Sea Ice and Coastal Waters, Annals of Glaciology, 3, 12–16,

729 doi:10.3189/S0260305500002445, 1982.

730 Anderson, R. F., Ali, S., Bradtmiller, L. I., Nielsen, S. H. H., Fleisher, M. Q., Anderson, B. E. and Burckle, L.

731 H.: Wind-Driven Upwelling in the Southern Ocean and the Deglacial Rise in Atmospheric CO2, Science, 323,

732 1443–1448, doi:10.1126/science.1167441, 2009.

733 Armand, L. K. and Zielinski, U.: DIATOM SPECIES OF THE GENUS *RHIZOSOLENIA* FROM SOUTHERN

734 OCEAN SEDIMENTS: DISTRIBUTION AND TAXONOMIC NOTES, Diatom Research, 16(2), 259–294,

735 doi:10.1080/0269249X.2001.9705520, 2001.

736 Arrigo, K. R., Worthen, D. L., Lizotte, M. P., Dixon, P. and Dieckmann, G.: Primary Production in Antarctic Sea

737 Ice, Science, 276, 394–397, doi:10.1126/science.276.5311.394, 1997.

738 Barbara, L., Crosta, X., Schmidt, S. and Massé, G.: Diatoms and biomarkers evidence for major changes in sea

739 ice conditions prior the instrumental period in Antarctic Peninsula, Quaternary Science Reviews, 79, 99–110,

740 doi:10.1016/j.quascirev.2013.07.021, 2013.

741 Barbara, L., Crosta, X., Leventer, A., Schmidt, S., Etourneau, J., Domack, E. and Massé, G.: Environmental

742 responses of the Northeast Antarctic Peninsula to the Holocene climate variability, Paleoceanography, 31(1),

743 131–147, doi:10.1002/2015PA002785, 2016.

744 Bárcena, M. A., Gersonde, R., Ledesma, S., Fabrés, J., Calafat, A. M., Canals, M., Sierro, F. J. and Flores, J. A.:

745 Record of Holocene glacial oscillations in Bransfield Basin as revealed by siliceous microfossil assemblages,

746 Antarctic Science, 10(03), 269–285, doi:10.1017/S0954102098000364, 1998.

747 Belt, S. T.: Source-specific biomarkers as proxies for Arctic and Antarctic sea ice, Organic Geochemistry, 125,

748 277–298, doi:10.1016/j.orggeochem.2018.10.002, 2018.

749 Belt, S. T., Smik, L., Brown, T. A., Kim, J. H., Rowland, S. J., Allen, C. S., Gal, J. K., Shin, K. H., Lee, J. I. and

Taylor, K. W. R.: Source identification and distribution reveals the potential of the geochemical Antarctic sea ice proxy IPSO25, Nature Communications, 7, 1–10, doi:10.1038/ncomms12655, 2016.

Belt, S. T. T., Brown, T. A. A., Ampel, L., Cabedo-Sanz, P., Fahl, K., Kocis, J. J. J., Massé, G., Navarro-Rodriguez, A., Ruan, J. and Xu, Y.: An inter-laboratory investigation of the Arctic sea ice biomarker proxy IP25 in marine sediments: key outcomes and recommendations, Climate of the Past, 10(1), 155–166, doi:10.5194/cp-10-155-2014, 2014.

Bentley, M. J., Hodgson, D. A., Smith, J. A., Cofaigh, C. ., Domack, E. W., Larter, R. D., Roberts, S. J., Brachfeld, S., Leventer, A., Hjort, C., Hillenbrand, C.-D. and Evans, J.: Mechanisms of Holocene palaeoenvironmental change in the Antarctic Peninsula region, The Holocene, 19(1), 51–69, doi:10.1177/0959683608096603, 2009.

Bentley, M. J., Ó Cofaigh, C., Anderson, J. B., Conway, H., Davies, B., Graham, A. G. C., Hillenbrand, C.-D., Hodgson, D. A., Jamieson, S. S. R., Larter, R. D., Mackintosh, A., Smith, J. A., Verleyen, E., Ackert, R. P., Bart, P. J., Berg, S., Brunstein, D., Canals, M., Colhoun, E. A., Crosta, X., Dickens, W. A., Domack, E., Dowdeswell, J. A., Dunbar, R., Ehrmann, W., Evans, J., Favier, V., Fink, D., Fogwill, C. J., Glasser, N. F., Gohl, K., Golledge, N. R., Goodwin, I., Gore, D. B., Greenwood, S. L., Hall, B. L., Hall, K., Hedding, D. W., Hein, A. S., Hocking, E. P., Jakobsson, M., Johnson, J. S., Jomelli, V., Jones, R. S., Klages, J. P., Kristoffersen, Y., Kuhn, G., Leventer, A., Licht, K., Lilly, K., Lindow, J., Livingstone, S. J., Massé, G., McGlone, M. S., McKay, R. M., Melles, M., Miura, H., Mulvaney, R., Nel, W., Nitsche, F. O., O'Brien, P. E., Post, A. L., Roberts, S. J., Saunders, K. M., Selkirk, P. M., Simms, A. R., Spiegel, C., Stolldorf, T. D., Sugden, D. E., van der Putten, N., van Ommen, T., Verfaillie, D., Vyverman, W., Wagner, B., White, D. A., Witus, A. E. and Zwartz, D.: A community-based geological reconstruction of Antarctic Ice Sheet deglaciation since the Last Glacial Maximum, Quaternary Science Reviews, 100(August), 1–9, doi:10.1016/j.quascirev.2014.06.025, 2014.

Blunier, T. and Brook, E. J.: Timing of millennial-scale climate change in antarctica and greenland during the last glacial period, Science, 291(5501), 109–112, doi:10.1126/science.291.5501.109, 2001.

Boyer, T., Garcia, H. E., Locarnini, R. A., Zweng, M. M., Mishonov, A. V and Reagan, J. R.: Wolrd Ocean Atlas 2018., 2018.

Bracegirdle, T. J., Stephenson, D. B., Turner, J. and Phillips, T.: The importance of sea ice area biases in 21st century multimodel projections of Antarctic temperature and precipitation, Geophysical Research Letters, 42(24), 10,832-10,839, doi:10.1002/2015GL067055, 2015.

Bracegirdle, T. J., Colleoni, F., Abram, N. J., Bertler, N. A. N., Dixon, D. A., England, M., Favier, V., Fogwill, C. J., Fyfe, J. C., Goodwin, I., Goosse, H., Hobbs, W., Jones, J. M., Keller, E. D., Khan, A. L., Phipps, S. J.,

Raphael, M. N., Russell, J., Sime, L., Thomas, E. R., van den Broeke, M. R. and Wainer, I.: Back to the Future: Using Long-Term Observational and Paleo-Proxy Reconstructions to Improve Model Projections of Antarctic Climate, Geosciences, 9(6), 255, doi:10.3390/geosciences9060255, 2019.

Broecker, W. S.: Paleocean circulation during the Last Deglaciation: A bipolar seesaw?, Paleoceanography, 13(2), 119–121, doi:10.1029/97PA03707, 1998.

Buffen, A., Leventer, A., Rubin, A. and Hutchins, T.: Diatom assemblages in surface sediments of the northwestern Weddell Sea, Antarctic Peninsula, Marine Micropaleontology, 62(1), 7–30, doi:10.1016/J.MARMICRO.2006.07.002, 2007.

Butterworth, B. J. and Miller, S. D.: Air-sea exchange of carbon dioxide in the Southern Ocean and Antarctic marginal ice zone, Geophysical Research Letters, 43(13), 7223–7230, doi:10.1002/2016GL069581, 2016.

Butzin, M., Köhler, P. and Lohmann, G.: Marine radiocarbon reservoir age simulations for the past 50,000 years, Geophysical Research Letters, 44(16), 8473–8480, doi:10.1002/2017GL074688, 2017.

Cádiz Hernández, A.: Evidencia de cambios en la productividad marina a partir de testigos sedimentarios recuperados en Bahía Fildes (Maxwell Bay) y Costa de Palmer, Península Antártica durante los últimos ~ 1000 años, Universidad de Valparaíso., 2019.

Canals, M. and Amblas, D.: Seafloor kettle holes in Orleans Trough, Bransfield Basin, Antarctic Peninsula, Geological Society, London, Memoirs, 46(1), 313–314, doi:10.1144/M46.16, 2016a.

Canals, M. and Amblas, D.: The bundle: a mega-scale glacial landform left by an ice stream, Western Bransfield Basin, Geological Society, London, Memoirs, 46(1), 177–178, doi:10.1144/M46.157, 2016b.

Canals, M., Amblas, D. and Casamor, J. L.: Cross-shelf troughs in Central Bransfield Basin, Antarctic Peninsula, Geological Society, London, Memoirs, 46(1), 171–172, doi:10.1144/M46.138, 2016.

Cárdenas, P., Lange, C. B., Vernet, M., Esper, O., Srain, B., Vorrath, M.-E. M.-E., Ehrhardt, S., Müller, J., Kuhn, G., Arz, H. W. H. W. H. W., Lembke-Jene, L., Lamy, F. and Paola Cárdenas, Carina B. Lange, Maria Vernet, Oliver Esper, Benjamin Srain, Maria-Elena Vorrath, Sophie Ehrhardt, Juliane Müller, Gerhard Kuhn, Helge W.Arz, Lester Lembke-Jene, F. L.: Biogeochemical proxies and diatoms in surface sediments across the Drake Passage reflect oceanic domains and frontal systems in the region, Progress in Oceanography, 174, 72–88, doi:10.1016/j.pocean.2018.10.004, 2019.

Carrasco, J. F., Bozkurt, D. and Cordero, R. R.: A review of the observed air temperature in the Antarctic Peninsula. Did the warming trend come back after the early 21st hiatus?, Polar Science, 28, 100653, doi:10.1016/j.polar.2021.100653, 2021.

Cavalieri, D. J., Parkinson, C. L., Gloersen, P. and Zwally, H. J.: Sea Ice Concentrations from Nimbus-7 SMMR

812   and DMSP SSM/I-SSMIS Passive Microwave Data, Version 1, Boulder, Colorado USA,

813   doi:10.5067/8GQ8LZQVL0VL, 1996.

814   Chisholm, S. W.: Stirring times in the Southern Ocean, Nature, 407(6805), 685–686, doi:10.1038/35037696,

815   2000.

816   Clark, P. U., Shakun, J. D., Baker, P. A., Bartlein, P. J., Brewer, S., Brook, E., Carlson, A. E., Cheng, H.,

817   Kaufman, D. S., Liu, Z., Marchitto, T. M., Mix, A. C., Morrill, C., Otto-Bliesner, B. L., Pahnke, K., Russell, J.

818   M., Whitlock, C., Adkins, J. F., Blois, J. L., Clark, J., Colman, S. M., Curry, W. B., Flower, B. P., He, F.,

819   Johnson, T. C., Lynch-Stieglitz, J., Markgraf, V., McManus, J., Mitrovica, J. X., Moreno, P. I. and Williams, J.

820   W.: Global climate evolution during the last deglaciation, Proceedings of the National Academy of Sciences,

821   109(19), E1134–E1142, doi:10.1073/pnas.1116619109, 2012.

822   Collares, L. L., Mata, M. M., Kerr, R., Arigony-Neto, J. and Barbat, M. M.: Iceberg drift and ocean circulation

823   in the northwestern Weddell Sea, Antarctica, Deep Sea Research Part II: Topical Studies in Oceanography,

824   149(January 2019), 10–24, doi:10.1016/j.dsr2.2018.02.014, 2018.

825   Cook, A. J., Holland, P. R., Meredith, M. P., Murray, T., Luckman, A. and Vaughan, D. G.: Ocean forcing of

826   glacier retreat in the western Antarctic Peninsula, Science, 353(6296), 283–286, doi:10.1126/science.aae0017,

827   2016.

828   Couto, N., Martinson, D. G., Kohut, J. and Schofield, O.: Distribution of Upper Circumpolar Deep Water on the

829   warming continental shelf of the West Antarctic Peninsula, Journal of Geophysical Research: Oceans, 122(7),

830   5306–5315, doi:10.1002/2017JC012840, 2017.

831   Crosta, X., Kohfeld, K. E., Bostock, H. C., Chadwick, M., Du Vivier, A., Esper, O., Etourneau, J., Jones, J.,

832   Leventer, A., Müller, J., Rhodes, R. H., Allen, C. S., Ghadi, P., Lamping, N., Lange, C. B., Lawler, K.-A., Lund,

833   D., Marzocchi, A., Meissner, K. J., Menviel, L., Nair, A., Patterson, M., Pike, J., Prebble, J. G., Riesselman, C.,

834   Sadatzki, H., Sime, L. C., Shukla, S. K., Thöle, L., Vorrath, M.-E., Xiao, W. and Yang, J.: Antarctic sea ice over

835   the past 130,000 years, Part 1: A review of what proxy records tell us, EGUsphere [preprint],

836   doi:10.5194/egusphere-2022-99, 2022.

837   Denis, D., Crosta, X., Barbara, L., Massé, G., Renssen, H., Ther, O. and Giraudeau, J.: Sea ice and wind

838   variability during the Holocene in East Antarctica: insight on middle–high latitude coupling, Quaternary Science

839   Reviews, 29(27–28), 3709–3719, doi:10.1016/J.QUASCIREV.2010.08.007, 2010.

840   Domack, E., Leventer, A., Dunbar, R., Taylor, F., Brachfeld, S. and Sjunneskogs, C.: Chronology of the Palmer

841   Deep site, Antarctic Peninsula: a Holocene palaeoenvironmental reference for the circum-Antarctic, The

842   Holocene, 11(1), 1–9, doi:10.1191/095968301673881493, 2001.

843 Domack, E. W.: A Synthesis for Site 1098: Palmer Deep, in Proceedings of the Ocean Drilling Program, 178

844 Scientific Results, Ocean Drilling Program., 2002.

845 Ducklow, H. W., Erickson, M., Kelly, J., Montes-Hugo, M., Ribic, C. A., Smith, R. C., Stammerjohn, S. E. and

846 Karl, D. M.: Particle export from the upper ocean over the continental shelf of the west Antarctic Peninsula: A

847 long-term record, 1992–2007, Deep Sea Research Part II: Topical Studies in Oceanography, 55(18–19), 2118–

848 2131, doi:10.1016/j.dsr2.2008.04.028, 2008.

849 EPICA Community Members: Eight glacial cycles from an Antarctic ice core, Nature, 429(6992), 623–628,

850 doi:10.1038/nature02599, 2004.

851 EPICA Community Members: One-to-one coupling of glacial climate variability in Greenland and Antarctica,

852 Nature, 444(7116), 195–198, doi:10.1038/nature05301, 2006.

853 Escutia, C., DeConto, R., Dunbar, R., De Santis, L., Shevenell, A. and Nash, T.: Keeping an Eye on Antarctic

854 Ice Sheet Stability, Oceanography, 32(1), 32–46, doi:10.5670/oceanog.2019.117, 2019.

855 Esper, O. and Gersonde, R.: New tools for the reconstruction of Pleistocene Antarctic sea ice, Palaeogeography,

856 Palaeoclimatology, Palaeoecology, 399, 260–283, doi:10.1016/J.PALAEO.2014.01.019, 2014a.

857 Esper, O. and Gersonde, R.: Quaternary surface water temperature estimations: New diatom transfer functions

858 for the Southern Ocean, Palaeogeography, Palaeoclimatology, Palaeoecology, 414, 1–19,

859 doi:10.1016/J.PALAEO.2014.08.008, 2014b.

860 Esper, O., Gersonde, R. and Kadagies, N.: Diatom distribution in southeastern Pacific surface sediments and

861 their relationship to modern environmental variables, Palaeogeography, Palaeoclimatology, Palaeoecology,

862 287(1–4), 1–27, doi:10.1016/J.PALAEO.2009.12.006, 2010.

863 Etourneau, J., Collins, L. G., Willmott, V., Kim, J. H., Barbara, L., Leventer, A., Schouten, S., Sinninghe

864 Damsté, J. S., Bianchini, A., Klein, V., Crosta, X. and Massé, G.: Holocene climate variations in the western

865 Antarctic Peninsula: Evidence for sea ice extent predominantly controlled by changes in insolation and ENSO

866 variability, Climate of the Past, 9(4), 1431–1446, doi:10.5194/cp-9-1431-2013, 2013.

867 Etourneau, J., Sgubin, G., Crosta, X., Swingedouw, D., Willmott, V., Barbara, L., Houssais, M. N., Schouten, S.,

868 Damsté, J. S. S., Goosse, H., Escutia, C., Crespin, J., Massé, G. and Kim, J. H.: Ocean temperature impact on ice

869 shelf extent in the eastern Antarctic Peninsula, Nature Communications, 10(1), 8–15, doi:10.1038/s41467-018-

870 08195-6, 2019.

871 Fietz, S., Huguet, C., Rueda, G., Hambach, B. and Rosell-Melé, A.: Hydroxylated isoprenoidal GDGTs in the

872 Nordic Seas, Marine Chemistry, 152, 1–10, doi:10.1016/j.marchem.2013.02.007, 2013.

873 Fischer, H., Fundel, F., Ruth, U., Twarloh, B., Wegner, A., Udisti, R., Becagli, S., Castellano, E., Morganti, A.,

Severi, M., Wolff, E., Littot, G., Röthlisberger, R., Mulvaney, R., Hutterli, M. A., Kaufmann, P., Federer, U., Lambert, F., Bigler, M., Hansson, M., Jonsell, U., de Angelis, M., Boutron, C., Siggaard-Andersen, M.-L., Steffensen, J. P., Barbante, C., Gaspari, V., Gabrielli, P. and Wagenbach, D.: Reconstruction of millennial changes in dust emission, transport and regional sea ice coverage using the deep EPICA ice cores from the Atlantic and Indian Ocean sector of Antarctica, Earth and Planetary Science Letters, 260(1–2), 340–354, doi:10.1016/j.epsl.2007.06.014, 2007.

Fletcher, M.-S., Pedro, J., Hall, T., Mariani, M., Alexander, J. A., Beck, K., Blaauw, M., Hodgson, D. A., Heijnis, H., Gadd, P. S. and Lise-Pronovost, A.: Northward shift of the southern westerlies during the Antarctic Cold Reversal, Quaternary Science Reviews, 271, 107189, doi:10.1016/j.quascirev.2021.107189, 2021.

Gersonde, R. and Zielinski, U.: The reconstruction of late Quaternary Antarctic sea-ice distribution — the use of diatoms as a proxy for sea-ice, , 162, 263–286, doi:10.1016/S0031-0182(00)00131-0, 2000.

Gersonde, R., Crosta, X., Abelmann, A. and Armand, L.: Sea-surface temperature and sea ice distribution of the Southern Ocean at the EPILOG Last Glacial Maximum—a circum-Antarctic view based on siliceous microfossil records, Quaternary Science Reviews, 24(7–9), 869–896, doi:10.1016/J.QUASCIREV.2004.07.015, 2005.

Gloersen, P., Campbell, W. J., Cavalieri, D. J., Comiso, J. C., Parkinson, C. L. and Zwally, H. J.: Arctic and antarctic sea ice, 1978, Annals of Glaciology, 17, 149–154, 1993.

Gonçalves-Araujo, R., de Souza, M. S., Tavano, V. M. and Garcia, C. A. E.: Influence of oceanographic features on spatial and interannual variability of phytoplankton in the Bransfield Strait, Antarctica, Journal of Marine Systems, 142, 1–15, doi:10.1016/J.JMARSYS.2014.09.007, 2015.

Han, Z., Hu, C., Sun, W., Zhao, J., Pan, J., Fan, G. and Zhang, H.: Characteristics of particle fluxes in the Prydz Bay polynya, Eastern Antarctica, Science China Earth Sciences, 62(4), 657–670, doi:10.1007/s11430-018-9285-6, 2019.

Hellmer, H. H., Kauker, F., Timmermann, R., Determann, J. and Rae, J.: Twenty-first-century warming of a large Antarctic ice-shelf cavity by a redirected coastal current, Nature, 485(7397), 225–228, doi:10.1038/nature11064, 2012.

Heroy, D. C., Sjunneskog, C. and Anderson, J. B.: Holocene climate change in the Bransfield Basin, Antarctic Peninsula: evidence from sediment and diatom analysis, Antarctic Science, 20(01), 69–87, doi:10.1017/S0954102007000788, 2008.

Hillaire-Marcel, C. and de Vernal, A.: Proxies in Late Cenozoic Paleoceanography, edited by C. Hillaire-Marcel and A. de Vernal, Elsevier, Amsterdam., 2007.

Hofmann, E. E., Klinck, J. M., Lascara, C. M. and Smith, D. A.: Water mass distribution and circulation west of

the Antarctic Peninsula and including Bransfield Strait, pp. 61–80, American Geophysical Union (AGU)., 1996.

Hopmans, E. C., Weijers, J. W. H., Schefuß, E., Herfort, L., Sinninghe Damsté, J. S. and Schouten, S.: Variability in the Benguela Current upwelling system over the past 70,000 years, Earth and Planetary Science Letters, 224(1–2), 107–116, doi:10.1016/j.epsl.2004.05.012, 2004.

Huss, M. and Farinotti, D.: A high-resolution bedrock map for the Antarctic Peninsula, The Cryosphere, 8(4), 1261–1273, doi:10.5194/tc-8-1261-2014, 2014.

Ingólfsson, Ó., Hjort, C. and Humlum, O.: Glacial and Climate History of the Antarctic Peninsula since the Last Glacial Maximum, Arctic, Antarctic, and Alpine Research, 35(2), 175–186, doi:10.1657/1523-0430(2003)035[0175:GACHOT]2.0.CO;2, 2003.

IPCC: Summary for Policymakers, in Climate Change 2021_ The Physical Science Basis. Contribution of working Group I to the Sixth Assessment Report of the Intergovernmental Panel on Climate Change, edited by V. Masson-Delmotte, P. Zhai, H.-O. Pörtner, D. Roberts, J. Skea, P. R. Shukla, A. Pirani, W. Moufouma-Okia, C. Péan, R. Pidcock, S. Connors, J. B. R. Matthews, Y. Chen, X. Zhou, M. I. Gomis, E. Lonnoy, T. Maycock, M. Tignor, and T. Waterfield, p. 32, Cambridge University Press., 2021.

Jones, R. S., Johnson, J. S., Lin, Y., Mackintosh, A. N., Sefton, J. P., Smith, J. A., Thomas, E. R. and Whitehouse, P. L.: Stability of the Antarctic Ice Sheet during the pre-industrial Holocene, Nature Reviews Earth & Environment, 3(8), 500–515, doi:10.1038/s43017-022-00309-5, 2022.

Jouzel, J., Vaikmae, R., Petit, J. R., Martin, M., Duclos, Y., Stievenard, M., Lorius, C., Toots, M., Mélières, M. A., Burckle, L. H., Barkov, N. I. and Kotlyakov, V. M.: The two-step shape and timing of the last deglaciation in Antarctica, Climate Dynamics, 11(3), 151–161, doi:10.1007/BF00223498, 1995.

Kalanetra, K. M., Bano, N. and Hollibaugh, J. T.: Ammonia-oxidizing Archaea in the Arctic Ocean and Antarctic coastal waters, Environmental Microbiology, 11(9), 2434–2445, doi:10.1111/j.1462-2920.2009.01974.x, 2009.

Kim, D., Kim, D. Y., Kim, Y. J., Kang, Y. C. and Shim, J.: Downward fluxes of biogenic material in Bransfield Strait, Antarctica, Antarctic Science, 16(3), 227–237, doi:10.1017/S0954102004002032, 2004.

Kim, J.-H., van der Meer, J., Schouten, S., Helmke, P., Willmott, V., Sangiorgi, F., Koç, N., Hopmans, E. C. and Damsté, J. S. S.: New indices and calibrations derived from the distribution of crenarchaeal isoprenoid tetraether lipids: Implications for past sea surface temperature reconstructions, Geochimica et Cosmochimica Acta, 74(16), 4639–4654, doi:10.1016/j.gca.2010.05.027, 2010.

Kim, J.-H., Crosta, X., Willmott, V., Renssen, H., Bonnin, J., Helmke, P., Schouten, S. and Sinninghe Damsté, J. S.: Holocene subsurface temperature variability in the eastern Antarctic continental margin, Geophysical

936   Research Letters, 39(6), doi:10.1029/2012GL051157, 2012.

937   Klunder, M. B., Laan, P., De Baar, H. J. W., Middag, R., Neven, I. and Van Ooijen, J.: Dissolved Fe across the

938   Weddell Sea and Drake Passage: impact of DFe on nutrient uptake, Biogeosciences, 11(3), 651–669,

939   doi:10.5194/bg-11-651-2014, 2014.

940   Kyrmanidou, A., Vadman, K. J., Ishman, S. E., Leventer, A., Brachfeld, S., Domack, E. W. and Wellner, J. S.:

941   Late Holocene oceanographic and climatic variability recorded by the Perseverance Drift, northwestern Weddell

942   Sea, based on benthic foraminifera and diatoms, Marine Micropaleontology, 141, 10–22,

943   doi:10.1016/j.marmicro.2018.03.001, 2018.

944   Lamping, N., Müller, J., Esper, O., Hillenbrand, C., Smith, J. A. and Kuhn, G.: Highly branched isoprenoids

945   reveal onset of deglaciation followed by dynamic sea-ice conditions in the western Amundsen Sea, Antarctica,

946   Quaternary Science Reviews, 228, 106103, doi:10.1016/j.quascirev.2019.106103, 2020.

947   Lamping, N., Müller, J., Hefter, J., Mollenhauer, G., Haas, C., Shi, X., Vorrath, M.-E., Lohmann, G. and

948   Hillenbrand, C.-D.: Evaluation of lipid biomarkers as proxies for sea ice and ocean temperatures along the

949   Antarctic continental margin, Climate of the Past, 17(5), 2305–2326, doi:10.5194/cp-17-2305-2021, 2021.

950   Lamy, F.: The expedition PS97 of the research vessel POLARSTERN to the Drake Passage in 2016, Reports on

951   Polar and Marine Research, 7'01, 1–571, doi:10.2312/BzPM_0702_2016, 2016.

952   Lamy, F., Kaiser, J., Arz, H. W., Hebbeln, D., Ninnemann, U., Timm, O., Timmermann, A. and Toggweiler, J.

953   R.: Modulation of the bipolar seesaw in the Southeast Pacific during Termination 1, Earth and Planetary Science

954   Letters, 259(3–4), 400–413, doi:10.1016/j.epsl.2007.04.040, 2007.

955   Liu, R., Han, Z., Zhao, J., Zhang, H., Li, D., Ren, J., Pan, J. and Zhang, H.: Distribution and source of glycerol

956   dialkyl glycerol tetraethers (GDGTs) and the applicability of GDGT-based temperature proxies in surface

957   sediments of Prydz Bay, East Antarctica, Polar Research, 39, doi:10.33265/polar.v39.3557, 2020.

958   Locarnini, M., Mishonov, A., Baranova, O., Boyer, T., Zweng, M., Garcia, H., Reagan, J., Seidov, D., Weathers,

959   K., Paver, C. and Smolyar, I.: World Ocean Atlas 2018, Volume 1: Temperature. [online] Available from:

960   https://archimer.ifremer.fr/doc/00651/76338/, 2018.

961   Lü, X., Liu, X. L., Elling, F. J., Yang, H., Xie, S., Song, J., Li, X., Yuan, H., Li, N. and Hinrichs, K. U.:

962   Hydroxylated isoprenoid GDGTs in Chinese coastal seas and their potential as a paleotemperature proxy for

963   mid-to-low latitude marginal seas, Organic Geochemistry, 89–90, 31–43,

964   doi:10.1016/j.orggeochem.2015.10.004, 2015.

965   Martinson, D. G. and McKee, D. C.: Transport of warm Upper Circumpolar Deep Water onto the western

966   Antarctic Peninsula continental shelf, Ocean Science, 8(4), 433–442, doi:10.5194/os-8-433-2012, 2012.

Massé, G., Belt, S. T., Crosta, X., Schmidt, S., Snape, I., Thomas, D. N. and Rowland, S. J.: Highly branched isoprenoids as proxies for variable sea ice conditions in the Southern Ocean, Antarctic Science, 23(05), 487–498, doi:10.1017/S0954102011000381, 2011.

McClymont, E. L., Bentley, M. J., Hodgson, D. A., Spencer-Jones, C. L., Wardley, T., West, M. D., Croudace, I. W., Berg, S., Gröcke, D. R., Kuhn, G., Jamieson, S. S. R., Sime, L. and Phillips, R. A.: Summer sea-ice variability on the Antarctic margin during the last glacial period reconstructed from snow petrel (Pagodroma nivea) stomach-oil deposits, Climate of the Past, 18(2), 381–403, doi:10.5194/cp-18-381-2022, 2022.

Meredith, M. P. and King, J. C.: Rapid climate change in the ocean west of the Antarctic Peninsula during the second half of the 20th century, Geophysical Research Letters, 32(19), 1–5, doi:10.1029/2005GL024042, 2005.

Milliken, K. T., Anderson, J. B., Wellner, J. S., Bohaty, S. M. and Manley, P. L.: High-resolution Holocene climate record from Maxwell Bay, South Shetland Islands, Antarctica, Geological Society of America Bulletin, 121(11–12), 1711–1725, doi:10.1130/B26478.1, 2009.

Minzoni, R. T., Anderson, J. B., Fernandez, R. and Wellner, J. S.: Marine record of Holocene climate, ocean, and cryosphere interactions: Herbert Sound, James Ross Island, Antarctica, Quaternary Science Reviews, 129, 239–259, doi:10.1016/j.quascirev.2015.09.009, 2015.

Mollenhauer, G., Grotheer, H., Gentz, T., Bonk, E. and Hefter, J.: Standard operation procedures and performance of the MICADAS radiocarbon laboratory at Alfred Wegener Institute (AWI), Germany, Nuclear Instruments and Methods in Physics Research Section B: Beam Interactions with Materials and Atoms, 496, 45–51, doi:10.1016/j.nimb.2021.03.016, 2021.

Morigi, C., Capotondi, L., Giglio, F., Langone, L., Brilli, M., Turi, B. and Ravaioli, M.: A possible record of the Younger Dryas event in deep-sea sediments of the Southern Ocean (Pacific sector), in Palaeogeography, Palaeoclimatology, Palaeoecology, vol. 198, pp. 265–278, Elsevier B.V., 2003.

Mortlock, R. A. and Froelich, P. N.: A simple method for the rapid determination of biogenic opal in pelagic marine sediments, Deep Sea Research Part A, Oceanographic Research Papers, 36(9), 1415–1426, doi:10.1016/0198-0149(89)90092-7, 1989.

Müller, J., Wagner, A., Fahl, K., Stein, R., Prange, M. and Lohmann, G.: Towards quantitative sea ice reconstructions in the northern North Atlantic: A combined biomarker and numerical modelling approach, Earth and Planetary Science Letters, 306(3–4), 137–148, doi:10.1016/J.EPSL.2011.04.011, 2011.

Müller, P. J. and Schneider, R.: An automated leaching method for the determination of opal in sediments and particulate matter, Deep-Sea Research Part I, 40(3), 425–444, doi:https://doi.org/10.1016/0967-0637(93)90140-X, 1993.

998 Mulvaney, R., Abram, N. J., Hindmarsh, R. C. A., Arrowsmith, C., Fleet, L., Triest, J., Sime, L. C., Alemany, O.

999 and Foord, S.: Recent Antarctic Peninsula warming relative to Holocene climate and ice-shelf history, Nature,

1000 489(7414), 141–144, doi:10.1038/nature11391, 2012.

1001 Murray, A. E., Preston, C. M., Massana, R., Taylor, L. T., Blakis, A., Wu, K. and DeLong, E. F.: Seasonal and

1002 Spatial Variability of Bacterial and Archaeal Assemblages in the Coastal Waters near Anvers Island, Antarctica,

1003 Applied and Environmental Microbiology, 64(7), 2585–2595, doi:10.1128/AEM.64.7.2585-2595.1998, 1998.

1004 Nicholls, K. W., Østerhus, S., Makinson, K., Gammelsrød, T. and Fahrbach, E.: Ice-ocean processes over the

1005 continental shelf of the southern Weddell Sea, Antarctica: A review, Reviews of Geophysics, 47(3), RG3003,

1006 doi:10.1029/2007RG000250, 2009.

1007 Ó Cofaigh, C., Davies, B. J., Livingstone, S. J., Smith, J. A., Johnson, J. S., Hocking, E. P., Hodgson, D. A.,

1008 Anderson, J. B., Bentley, M. J., Canals, M., Domack, E., Dowdeswell, J. A., Evans, J., Glasser, N. F.,

1009 Hillenbrand, C.-D., Larter, R. D., Roberts, S. J. and Simms, A. R.: Reconstruction of ice-sheet changes in the

1010 Antarctic Peninsula since the Last Glacial Maximum, Quaternary Science Reviews, 100, 87–110,

1011 doi:10.1016/j.quascirev.2014.06.023, 2014.

1012 Oksanen, J., Blanchet, F. G., Kindt, R., Legendre, P., Minchin, P. R., O´Hara, R. B., Simpson, G. L., Solymos,

1013 P., Stevens, M. H. H. and Wagner, H.: Vegan: Community Ecology Package (R Package Version 2.0-3), 2012.

1014 Parkinson, C. L. and Cavalieri, D. J.: Antarctic sea ice variability and trends, 1979–2010, The Cryosphere, 6,

1015 871–880, doi:10.5194/tc-6-871-2012, 2012.

1016 Pedro, J. B., Bostock, H. C., Bitz, C. M., He, F., Vandergoes, M. J., Steig, E. J., Chase, B. M., Krause, C. E.,

1017 Rasmussen, S. O., Markle, B. R. and Cortese, G.: The spatial extent and dynamics of the Antarctic Cold

1018 Reversal, Nature Geoscience, 9(1), 51–55, doi:10.1038/ngeo2580, 2016.

1019 QGIS, D. T.: QGIS Geographic Information System, [online] Available from: http://qgis.osgeo.org, 2018.

1020 R Core Team: R: a Language and Environment for Statistical Computing, R Foundation for Statistical

1021 computing, Vienna., 2012.

1022 Reimer, P. J., Austin, W. E. N., Bard, E., Bayliss, A., Blackwell, P. G., Bronk Ramsey, C., Butzin, M., Cheng,

1023 H., Edwards, R. L., Friedrich, M., Grootes, P. M., Guilderson, T. P., Hajdas, I., Heaton, T. J., Hogg, A. G.,

1024 Hughen, K. A., Kromer, B., Manning, S. W., Muscheler, R., Palmer, J. G., Pearson, C., van der Plicht, J.,

1025 Reimer, R. W., Richards, D. A., Scott, E. M., Southon, J. R., Turney, C. S. M., Wacker, L., Adolphi, F.,

1026 Büntgen, U., Capano, M., Fahrni, S. M., Fogtmann-Schulz, A., Friedrich, R., Köhler, P., Kudsk, S., Miyake, F.,

1027 Olsen, J., Reinig, F., Sakamoto, M., Sookdeo, A. and Talamo, S.: The IntCal20 Northern Hemisphere

1028 Radiocarbon Age Calibration Curve (0–55 cal kBP), Radiocarbon, 62(4), 725–757, doi:10.1017/RDC.2020.41,

1029   2020.

1030   Reynolds, R. W., Rayner, N. A., Smith, T. M., Stokes, D. C., Wang, W., Reynolds, R. W., Rayner, N. A., Smith,

1031   T. M., Stokes, D. C. and Wang, W.: An Improved In Situ and Satellite SST Analysis for Climate, Journal of

1032   Climate, 15(13), 1609–1625, doi:10.1175/1520-0442(2002)015<1609:AIISAS>2.0.CO;2, 2002.

1033   Reynolds, R. W., Smith, T. M., Liu, C., Chelton, D. B., Casey, K. S., Schlax, M. G., Reynolds, R. W., Smith, T.

1034   M., Liu, C., Chelton, D. B., Casey, K. S. and Schlax, M. G.: Daily High-Resolution-Blended Analyses for Sea

1035   Surface Temperature, Journal of Climate, 20(22), 5473–5496, doi:10.1175/2007JCLI1824.1, 2007.

1036   Rignot, E., Mouginot, J., Scheuchl, B., van den Broeke, M., van Wessem, M. J. and Morlighem, M.: Four

1037   decades of Antarctic Ice Sheet mass balance from 1979–2017, Proceedings of the National Academy of

1038   Sciences, 116(4), 1095–1103, doi:10.1073/pnas.1812883116, 2019.

1039   Roche, D. M., Crosta, X. and Renssen, H.: Evaluating Southern Ocean sea-ice for the Last Glacial Maximum

1040   and pre-industrial climates: PMIP-2 models and data evidence, Quaternary Science Reviews, 56, 99–106,

1041   doi:10.1016/j.quascirev.2012.09.020, 2012.

1042   Ronge, T. A., Lippold, J., Geibert, W., Jaccard, S. L., Mieruch-Schnülle, S., Süfke, F. and Tiedemann, R.:

1043   Deglacial patterns of South Pacific overturning inferred from 231Pa and 230Th, Scientific Reports, 11(1),

1044   doi:10.1038/s41598-021-00111-1, 2021.

1045   Roseby, Z. A., Smith, J. A., Hillenbrand, C.-D., Cartigny, M. J. B., Rosenheim, B. E., Hogan, K. A., Allen, C.

1046   S., Leventer, A., Kuhn, G., Ehrmann, W. and Larter, R. D.: History of Anvers-Hugo Trough, western Antarctic

1047   Peninsula shelf, since the Last Glacial Maximum. Part I: Deglacial history based on new sedimentological and

1048   chronological data, Quaternary Science Reviews, 291, 107590, doi:10.1016/j.quascirev.2022.107590, 2022.

1049   Ruiz Barlett, E. M., Tosonotto, G. V., Piola, A. R., Sierra, M. E. and Mata, M. M.: On the temporal variability of

1050   intermediate and deep waters in the Western Basin of the Bransfield Strait, Deep Sea Research Part II: Topical

1051   Studies in Oceanography, 149, 31–46, doi:10.1016/j.dsr2.2017.12.010, 2018.

1052   Sangrà, P., Gordo, C., Hernández-Arencibia, M., Marrero-Díaz, A., Rodríguez-Santana, A., Stegner, A.,

1053   Martínez-Marrero, A., Pelegrí, J. L. and Pichon, T.: The Bransfield current system, Deep Sea Research Part I:

1054   Oceanographic Research Papers, 58(4), 390–402, doi:10.1016/J.DSR.2011.01.011, 2011.

1055   Sangrà, P., Stegner, A., Hernández-Arencibia, M., Marrero-Díaz, Á., Salinas, C., Aguiar-González, B.,

1056   Henríquez-Pastene, C. and Mouriño-Carballido, B.: The Bransfield Gravity Current, Deep-Sea Research Part I:

1057   Oceanographic Research Papers, 119(November 2016), 1–15, doi:10.1016/j.dsr.2016.11.003, 2017.

1058   Scherer, R. P.: A new method for the determination of absolute abundance of diatoms and other silt-sized

1059   sedimentary particles, Journal of Paleolimnology, 12(2), 171–179, doi:10.1007/BF00678093, 1994.

1060   Schlüter, M. and Rickert, D.: Effect of pH on the measurement of biogenic silica, Marine Chemistry, 63(1–2),

1061   81–92, doi:10.1016/S0304-4203(98)00052-8, 1998.

1062   Schofield, O., Brown, M., Kohut, J., Nardelli, S., Saba, G., Waite, N. and Ducklow, H.: Changes in the upper

1063   ocean mixed layer and phytoplankton productivity along the West Antarctic Peninsula, Philosophical

1064   Transactions of the Royal Society A: Mathematical, Physical and Engineering Sciences, 376(2122),

1065   doi:10.1098/rsta.2017.0173, 2018.

1066   Schrader, H. and Gersonde, R.: Diatoms and silicoflagellates, in Micropaleontological Methods and Techniques

1067   - An Excercise on an Eight Meter Section of the Lower Pliocene of Capo Rossello, Sicily, Utrecht

1068   Micropaleontological Bulletins, vol. 17, edited by W. J. Zachariasse, W. R. Riedel, A. Sanfilippo, R. R. Schmidt,

1069   M. J. Brolsma, H. J. Schrader, R. Gersonde, M. M. Drooger, and J. A. Broekman, pp. 129–176., 1978.

1070   Shevenell, A. E., Ingalls, A. E., Domack, E. W. and Kelly, C.: Holocene Southern Ocean surface temperature

1071   variability west of the Antarctic Peninsula, Nature, 470(7333), 250–254, doi:10.1038/nature09751, 2011.

1072   Simpson, G. L. and Oksanen, J.: Analogue: Analogue Matching and Modern Analogue Technique Transfer

1073   Function Models. R Package Version 0.8-2, 2012.

1074   Sjunneskog, C. and Taylor, F.: Postglacial marine diatom record of the Palmer Deep, Antarctic Peninsula (ODP

1075   Leg 178, Site 1098) 1. Total diatom abundance, Paleoceanography, 17(3), PAL 4-1-PAL 4-8,

1076   doi:10.1029/2000PA000563, 2002.

1077   Stenni, B., Masson-Delmotte, V., Johnsen, S., Jouzel, J., Longinelli, A., Monnin, E., Röthlisberger, R. and

1078   Selmo, E.: An Oceanic Cold Reversal During the Last Deglaciation, Science, 293(5537), 2074–2077,

1079   doi:10.1126/science.1059702, 2001.

1080   Stuiver, M., Reimer, P. J. and Reimer, R. W.: Calib 7.1, [online] Available from: http://calib.org/ (Accessed 20

1081   November 2021), 2018.

1082   Thomas, Allen, Etourneau, King, Severi, Winton, Mueller, Crosta and Peck: Antarctic Sea Ice Proxies from

1083   Marine and Ice Core Archives Suitable for Reconstructing Sea Ice over the past 2000 Years, Geosciences, 9(12),

1084   506, doi:10.3390/geosciences9120506, 2019.

1085   Timmermann, A., Okumura, Y., An, S.-I., Clement, A., Dong, B., Guilyardi, E., Hu, A., Jungclaus, J. H.,

1086   Renold, M., Stocker, T. F., Stouffer, R. J., Sutton, R., Xie, S.-P. and Yin, J.: The Influence of a Weakening of the

1087   Atlantic Meridional Overturning Circulation on ENSO, Journal of Climate, 20(19), 4899–4919,

1088   doi:10.1175/JCLI4283.1, 2007.

1089   Totten, R. L., Fonseca, A. N. R., Wellner, J. S., Munoz, Y. P., Anderson, J. B., Tobin, T. S. and Lehrmann, A.

1090   A.: Oceanographic and climatic influences on Trooz Glacier, Antarctica during the Holocene, Quaternary

1091 Science Reviews, 276, 107279, doi:10.1016/j.quascirev.2021.107279, 2022.

1092 Turner, J., Orr, A., Gudmundsson, G. H., Jenkins, A., Bingham, R. G., Hillenbrand, C.-D. and Bracegirdle, T. J.:

1093 Atmosphere-ocean-ice interactions in the Amundsen Sea Embayment, West Antarctica, Reviews of Geophysics,

1094 55(1), 235–276, doi:10.1002/2016RG000532, 2017.

1095 Vancoppenolle, M., Meiners, K. M., Michel, C., Bopp, L., Brabant, F., Carnat, G., Delille, B., Lannuzel, D.,

1096 Madec, G., Moreau, S., Tison, J. L. and van der Merwe, P.: Role of sea ice in global biogeochemical cycles:

1097 Emerging views and challenges, Quaternary Science Reviews, 79, 207–230,

1098 doi:10.1016/j.quascirev.2013.04.011, 2013.

1099 Vaughan, D. G., Marshall, G. J., Connolley, W. M., Parkinson, C., Mulvaney, R., Hodgson, D. A., King, J. C.,

1100 Pudsey, C. J. and Turner, J.: Recent Rapid Regional Climate Warming on the Antarctic Peninsula, Climatic

1101 Change, 60(3), 243–274, doi:10.1023/A:1026021217991, 2003.

1102 Vernet, M., Martinson, D., Iannuzzi, R., Stammerjohn, S., Kozlowski, W., Sines, K., Smith, R. and Garibotti, I.:

1103 Primary production within the sea-ice zone west of the Antarctic Peninsula: I—Sea ice, summer mixed layer,

1104 and irradiance, Deep Sea Research Part II: Topical Studies in Oceanography, 55(18–19), 2068–2085,

1105 doi:10.1016/j.dsr2.2008.05.021, 2008.

1106 Vorrath, M.-E., Müller, J., Esper, O., Mollenhauer, G., Haas, C., Schefuß, E. and Fahl, K.: Highly branched

1107 isoprenoids for Southern Ocean sea ice reconstructions: a pilot study from the Western Antarctic Peninsula,

1108 Biogeosciences, 16(15), 2961–2981, doi:10.5194/bg-16-2961-2019, 2019.

1109 Vorrath, M.-E., Müller, J., Rebolledo, L., Cárdenas, P., Shi, X., Esper, O., Opel, T., Geibert, W., Muñoz, P.,

1110 Haas, C., Kuhn, G., Lange, C. B., Lohmann, G. and Mollenhauer, G.: Sea ice dynamics in the Bransfield Strait,

1111 Antarctic Peninsula, during the past 240 years: a multi-proxy intercomparison study, Climate of the Past, 16(6),

1112 2459–2483, doi:10.5194/cp-16-2459-2020, 2020.

1113 WAIS Divide Project Members: Onset of deglacial warming in West Antarctica driven by local orbital forcing,

1114 Nature, 500(7463), 440–444, doi:10.1038/nature12376, 2013.

1115 WAIS Divide Project Members: Precise interpolar phasing of abrupt climate change during the last ice age,

1116 Nature, 520(7549), 661–665, doi:10.1038/nature14401, 2015.

1117 Warnock, J. P. and Scherer, R. P.: A revised method for determining the absolute abundance of diatoms, Journal

1118 of Paleolimnology, 53(1), 157–163, doi:10.1007/s10933-014-9808-0, 2015.

1119 Wefer, G., Fischer, G., Füetterer, D. and Gersonde, R.: Seasonal particle flux in the Bransfield Strait, Antartica,

1120 Deep Sea Research Part A. Oceanographic Research Papers, 35(6), 891–898, doi:10.1016/0198-0149(88)90066-

1121 0, 1988.

1122 Wu, S., Kuhn, G., Diekmann, B., Lembke-Jene, L., Tiedemann, R., Zheng, X., Ehrhardt, S., Arz, H. W. and

1123 Lamy, F.: Surface sediment characteristics related to provenance and ocean circulation in the Drake Passage

1124 sector of the Southern Ocean, Deep Sea Research Part I: Oceanographic Research Papers, 154, 103135,

1125 doi:10.1016/j.dsr.2019.103135, 2019.

1126 Zielinski, U. and Gersonde, R.: Diatom distribution in Southern Ocean surface sediments (Atlantic sector):

1127 Implications for paleoenvironmental reconstructions, Palaeogeography, Palaeoclimatology, Palaeoecology,

1128 129(3–4), 213–250, doi:10.1016/S0031-0182(96)00130-7, 1997.

1129 Zwally, H. J., Comiso, J. C., Parkinson, C. L., Cavalieri, D. J. and Gloersen, P.: Variability of Antarctic sea ice

1130 1979–1998, Journal of Geophysical Research, 107(C5), 3041, doi:10.1029/2000JC000733, 2002.

1131

1132

Figures
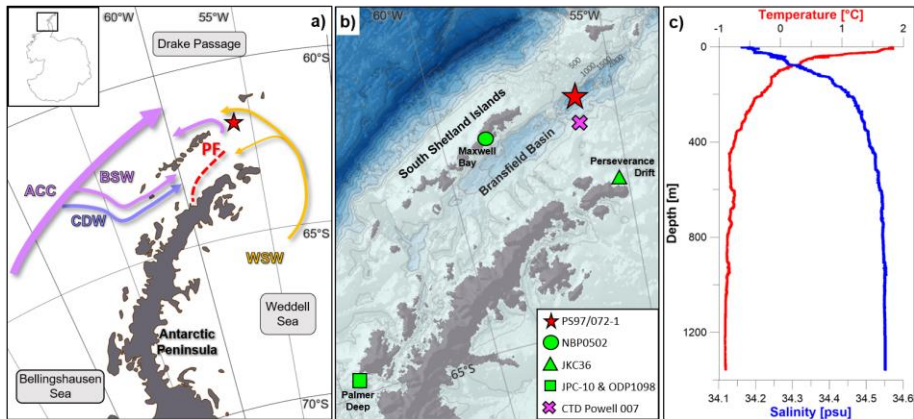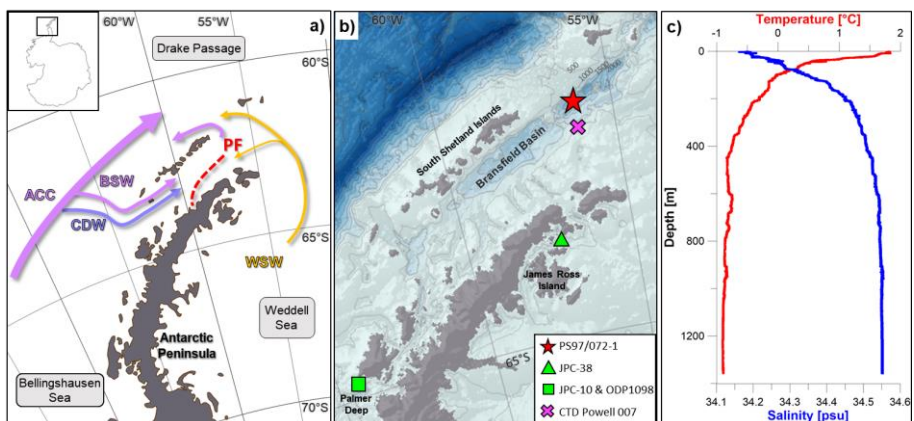
Figure 1: a) Overview map with modern oceanography in the study area (Hofmann et al., 1996; Sangrà et al., 2011). ACC = Antarctic Circumpolar Current, BSW = Bellingshausen Sea Water, CDW = Circumpolar Deep Water, WSW = Weddell Sea Water, and PF = Peninsula Front. b) Bathymetric features in the Bransfield Strait with the location of sediment core PS97/072-1 (red star) and other sediment records discussed in the text (green), and the CTD station (purple cross) where c) the vertical profile of ocean temperature and salinity (cruise POWELL2020, CTD 007 (62°09.075'S, 56°37.09'W) from 27.01.2020) shows a clear stratification of the upper 100 m of the water column. It indicates that surface waters are dominated by the BSW, while the basin is filled with WSW water. Maps were done with QGIS 3.0 (QGIS, 2018)and the bathymetry was taken from GEBCO_14 from 2015.
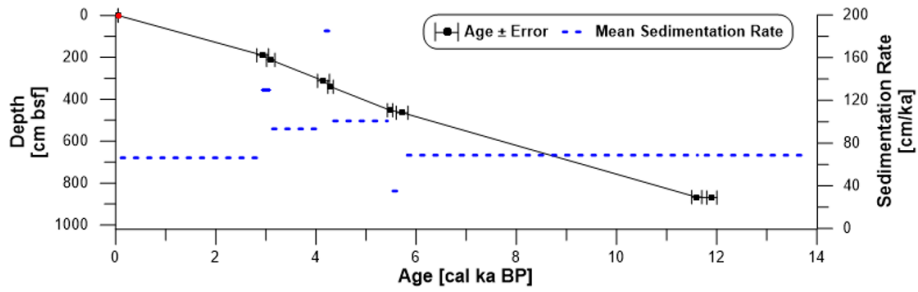
1146   Figure 2: Age-depth model for sediment core PS97/072-1 based on eight ^{14}C dated calcite samples (black) with

1147   error bars and mean sedimentation rates (cm/ka, dashed blue line). The core top age (red) was estimated as 0.05

1148   ka BP from matching with the ^{210}Pb-dated multicore PS97/072-2 (Vorrath et al., 2020; see supplement section 2).

1149

1150
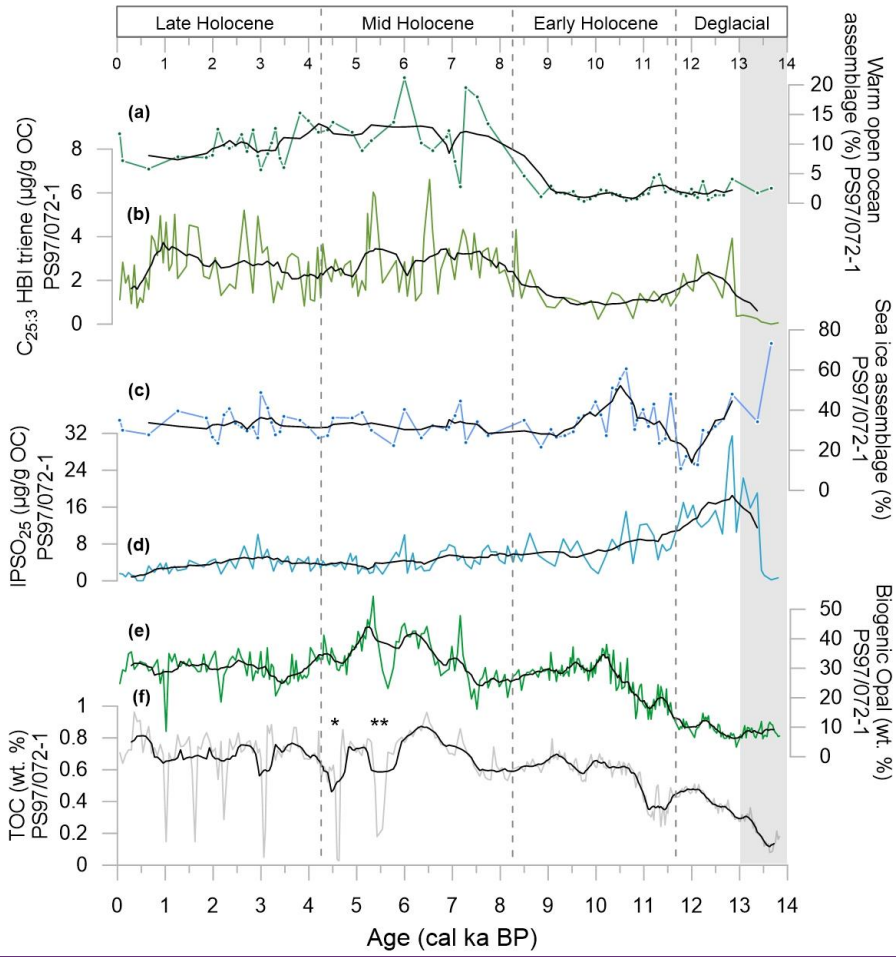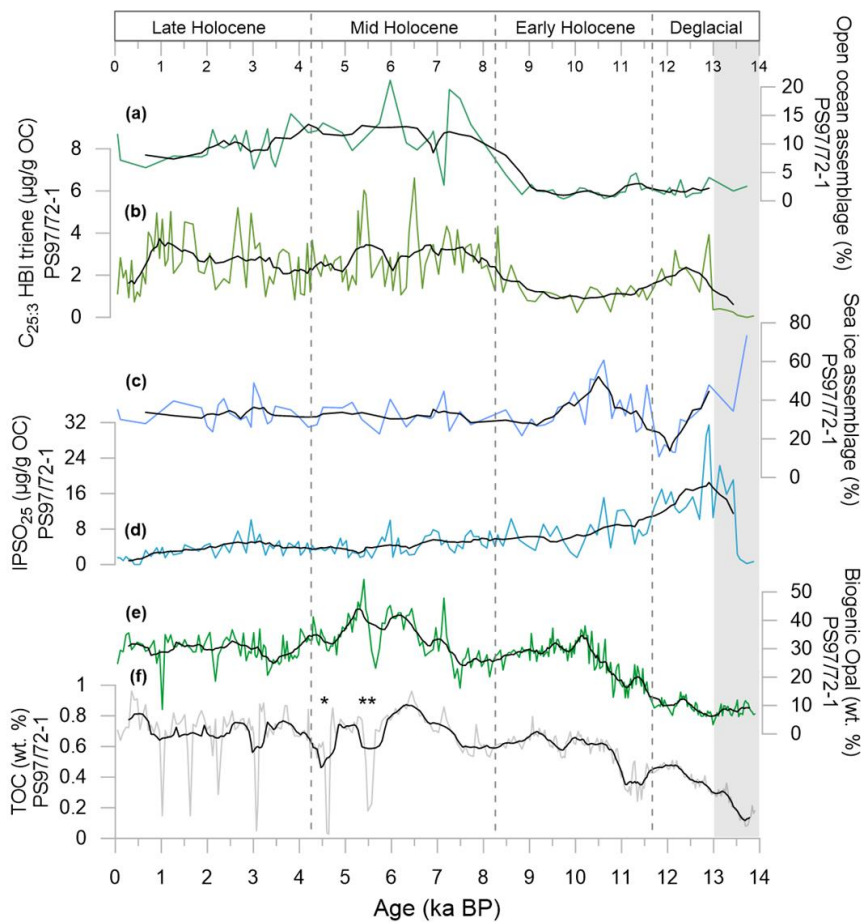
Figure 3: Overview of organic geochemical parameters and main diatom assemblages determined in sediment core PS97/072-1 used to characterize the environmental setting over the past 14 ka BP. a) warm open ocean diatom assemblage, b) $C_{25:3}$ HBI triene, c) sea ice diatom assemblage, d) $IPSO_{25}$, e) biogenic opal and f) TOC contents. Asterisks in f) mark layers of volcanic ash, where ** can be linked to a tephra layer in a sediment core from the Bransfield Strait at 5.5 ka BP (Heroy et al., 2008). Black lines display running averages. Grey shaded interval refers to the Antarctic Cold Reversal.

1162
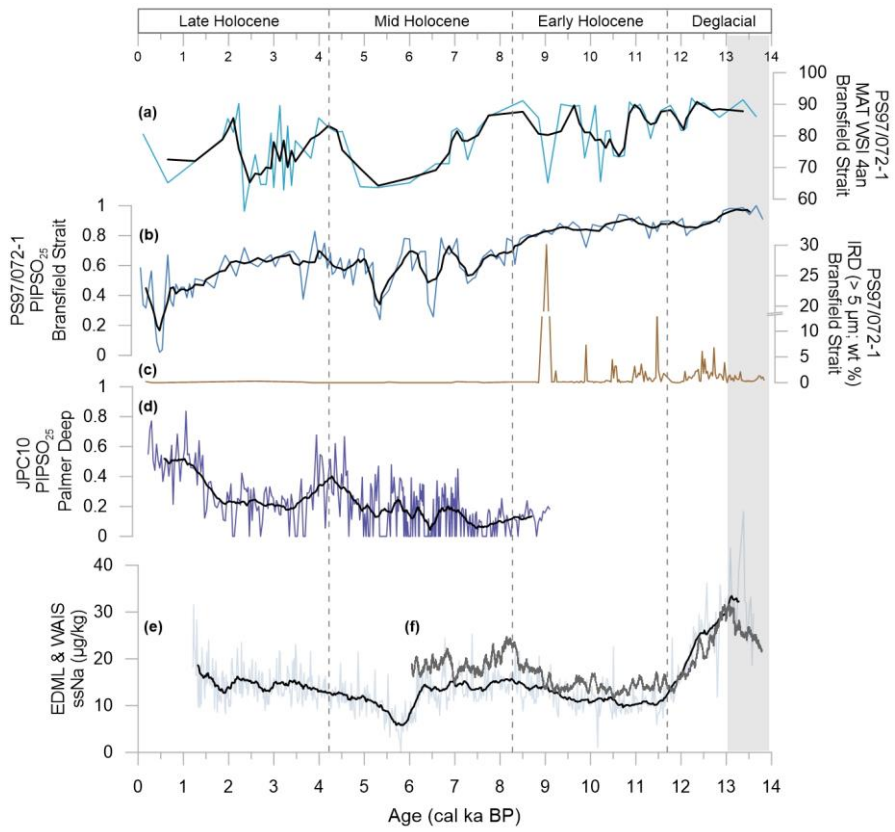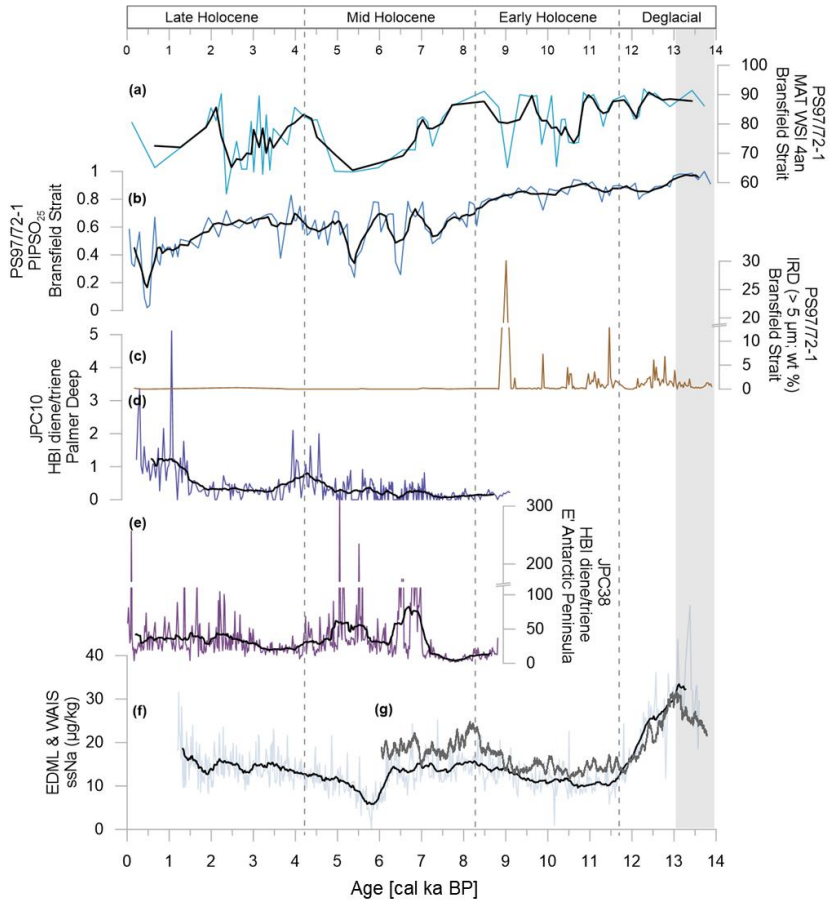
1163 Figure 4: Sea ice related proxies in sediment core PS97/072-1 with a) the diatom based WSI, b) the sea ice index

1164 PIPSO$_{25}$, and c) ice rafted debris (IRD). For comparison: PIPSO$_{25}$ values the HBI diene/triene ratio of sediment

1165 core d) JPC10 from the Palmer Deep station (Etourneau et al., 2013) and e) JPC38 at the East Antarctic Peninsula

1166 (Barbara et al., 2016). ssNa records of ef) the EDML ice core (Fischer et al., 2007) and fg) the WAIS ice core

1167 (WAIS Divide Project Members, 2015). Black lines display running averages. Grey shaded interval refers to the

1168 Antarctic Cold ReversalCR.

1169

1170

1172

Figure 5: A comparison of a) December insolation (Laskar et al., 2004), b) diatom-based SSST, c) RI-OH'-derived

SOT, d) September Spring insolation (Laskar et al., 2004), e) TEX_{86}^L-SOT of sediment core PS97/072-1, and

temperature reconstructions fe) TEX_{86}^L from JPC10, Palmer Deep (Etourneau et al., 2013), gd) TEX_{86} from

ODP1098, Palmer Deep (Shevenell et al., 2011), e) TEX_{86}^L from JPC38, East Antarctic Peninsula, and h) ice core

stable isotope records of h) JRI (Mulvaney et al., 2012), and i) WAIS Divide (WAIS Divide Project Members,

2013). Ocean temperatures are displayed as anomalies with respect to the mean of the individual SOT and SSST

1179   values of the entire record. Black lines display running averages. Grey shaded area refers to the Antarctic Cold

1180   Reversal.

1181